Title
Coordinate control of basal epithelial cell fate and stem cell maintenance by core EMT transcription factor Zeb1

Journal
Cell Reports, 38(2)

ISSN
2639-1856

Authors
Han, Yingying
Villarreal-Ponce, Alvaro
Gutierrez, Guadalupe
et al.

Publication Date
2022

DOI
10.1016/j.celrep.2021.110240

Peer reviewed

HHS Public Access

Author manuscript

Cell Rep. Author manuscript; available in PMC 2023 February 02.

Published in final edited form as:

Cell Rep. 2022 January 11; 38(2): 110240. doi:10.1016/j.celrep.2021.110240.

Coordinate control of basal epithelial cell fate and stem cell maintenance by core EMT transcription factor Zeb1

Yingying Han[1,7], **Alvaro Villarreal-Ponce**[1,7], **Guadalupe Gutierrez Jr.**[1], **Quy Nguyen**[1], **Peng Sun**[1], **Ting Wu**[2], **Benjamin Sui**[1], **Geert Berx**[3,4], **Thomas Brabletz**[5], **Kai Kessenbrock**[1], **Yi Arial Zeng**[2], **Kazuhide Watanabe**[1,6], **Xing Dai**[1,8,*]

[1]Department of Biological Chemistry, School of Medicine, D250 Med Sci I, University of California, Irvine, Irvine, CA 92697-1700, USA

[2]Institute of Biochemistry and Cell Biology, Shanghai Institutes for Biological Sciences, Chinese Academy of Sciences, 320 Yue-yang Road, Shanghai 200031, China

[3]Molecular and Cellular Oncology Lab, Department of Biomedical Molecular Biology, Ghent University, Technologiepark 71, 9052 Zwijnaarde, Belgium

[4]Cancer Research Institute Ghent, Ghent, Belgium

[5]Department of Experimental Medicine, Nikolaus-Fiebiger-Center for Molecular Medicine I, University, Erlangen-Nuernberg Glueckstr. 6, 91054 Erlangen, Germany

[6]RIKEN Center for Integrative Medical Sciences, Yokohama 230-0045, Japan

[7]These authors contributed equally

[8]Lead contact

SUMMARY

Maintenance of undifferentiated, long-lived, and often quiescent stem cells in the basal compartment is important for homeostasis and regeneration of multiple epithelial tissues, but the molecular mechanisms that coordinately control basal cell fate and stem cell quiescence are elusive. Here, we report an epithelium-intrinsic requirement for *Zeb1*, a core transcriptional inducer of epithelial-to-mesenchymal transition, for mammary epithelial ductal side branching and for basal cell regenerative capacity. Our findings uncover an evolutionarily conserved role of *Zeb1* in promoting basal cell fate over luminal differentiation. We show that *Zeb1* loss results in increased basal cell proliferation at the expense of quiescence and self-renewal. Moreover, *Zeb1* cooperates with YAP to activate *Axin2* expression, and inhibition of Wnt signaling partially

*Correspondence: xdai@uci.edu.

AUTHOR CONTRIBUTIONS

X.D. conceived the study and directed the project. Y.H., A.V.-P., T.W., Y.A.Z., K.W., and X.D. designed and Y.H., A.V.-P., Q.N., P.S., T.W., and K.W. performed the experiments. K.K. provided guidance on scRNA-seq, and G.G. and B.S. analyzed the single cell data. G.B. and T.B. provided the *Zeb1* floxed allele. X.D., A.V.-P., and Y.H. wrote the manuscript with input from all authors.

SUPPLEMENTAL INFORMATION

Supplemental information can be found online at https://doi.org/10.1016/j.celrep.2021.110240.

DECLARATION OF INTERESTS

The authors declare no competing interests.

restores stem cell function to *Zeb1*-deficient basal cells. Thus, *Zeb1* is a transcriptional regulator that maintains both basal cell fate and stem cell quiescence, and it functions in part through suppressing Wnt signaling.

In brief

Maintenance of undifferentiated, long-lived, and often quiescent stem cells in the basal compartment is important for homeostasis and regeneration of myriad epithelial tissues. Han et al. report a mammary epithelium-intrinsic mechanism involving *Zeb1*, known for its role in epithelial-mesenchymal plasticity, that regulates both basal cell fate and stem cell quiescence.

Graphical Abstract

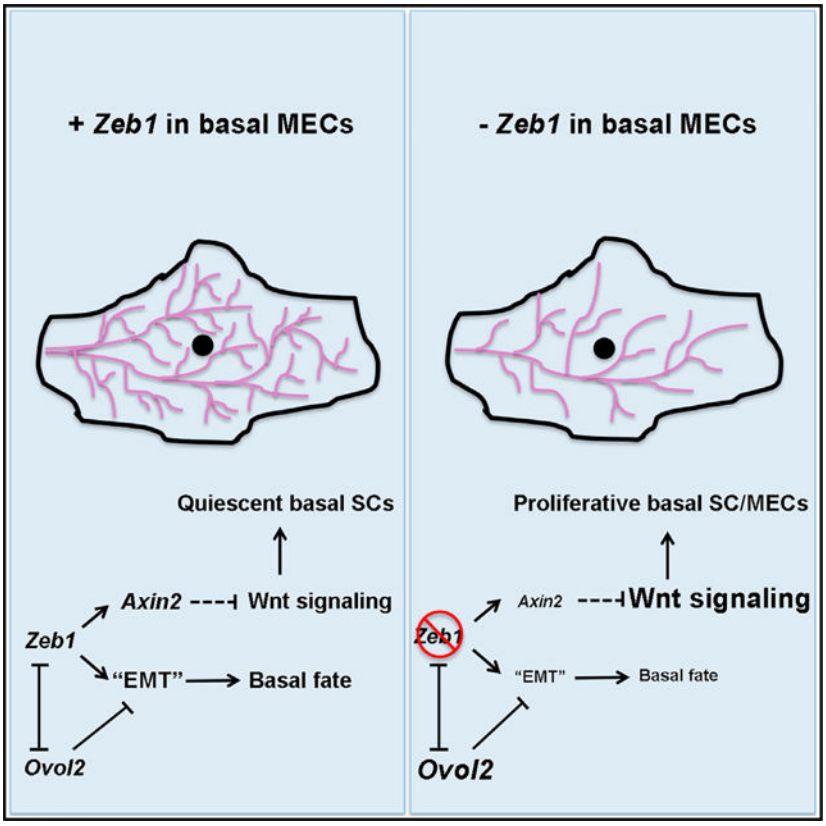

INTRODUCTION

Mammary gland (MG) morphogenesis initiates during embryogenesis, but the vast formation and remodeling of its complex epithelial ductal architecture occur postnatally during the stages of puberty, estrus cycle, and pregnancy (Fu et al., 2020; Inman et al., 2015; Watson and Khaled, 2008, 2020). Growth and maintenance of the bi-lineage mammary epithelium is dependent on the activity of stem cells (SCs) that reside in the outer basal compartment, which produce either only basal/myoepithelial progeny cells (unipotent SCs) or both basal/myoepithelial and inner luminal progeny cells (multi/bi-potent SCs; Van Amerongen et al., 2012; Van Keymeulen et al., 2011; Lloyd-Lewis et al., 2018;

Prater et al., 2014; Rios et al., 2014; Shackleton et al., 2006; Stingl et al., 2006; Wang et al., 2015; Wuidart et al., 2016). Mammary basal SCs are also responsible for fueling the regeneration of a new ductal network upon cleared fat pad transplantation (Prater et al., 2014; Shackleton et al., 2006; Stingl et al., 2006). Increasing evidence indicates that basal SCs are heterogeneous and encompass multiple diverse subsets, including the *Lgr5*$^{+}$ *Tspan8*^{high} basal cells and *Bcl11b*^{high} basal cells that are spatially distinct but both display quiescent features (Cai et al., 2017; Fu et al., 2017, 2020; Watson, 2021). However, the molecular mechanisms that coordinately control SC activities, such as quiescence and proliferation, with basal cell characteristics remain largely elusive.

Epithelial-to-mesenchymal transition (EMT) describes a heterogeneous spectrum of cellular plasticity, where epithelial cells lose or attenuate their epithelial traits and gain partial or complete mesenchymal characteristics (Haensel and Dai, 2018; Nieto et al., 2016; Pastushenko and Blanpain, 2019; Sha et al., 2019; Thiery et al., 2009; Yang et al., 2020). In breast cancer cells, expression of core EMT-associated transcription factors (EMT-TFs) belonging to the Snail, Twist, and Zeb families is linked to the acquisition of SC traits (Chaffer et al., 2013; Guo et al., 2012; Mani et al., 2008; Morel et al., 2008; Stemmler et al., 2019; Yang et al., 2004). However, whether EMT-TFs play physiological roles in maintaining epithelial tissue SCs and in promoting the “quasi-mesenchymal” mammary basal cell state (Lim et al., 2010; Nassour et al., 2012; Sikandar et al., 2017; Ye et al., 2015) remains enigmatic, as studies focused on understanding the significance of EMT-TFs in mammary epithelial SCs have produced discordant findings (Ballard et al., 2015; Fu et al., 2019, 2020; Guo et al., 2012; Nassour et al., 2012; Sikandar et al., 2017; Ye et al., 2015). *Zeb1/ZEB1* has emerged as a candidate regulator of basal SCs, given its elevated expression in Procr^{+}, cycling basal multipotent SCs (Wang et al., 2015), and in human breast basal epithelial stem/progenitor cells (Nguyen et al., 2018). However, functional evidence for *Zeb1/ ZEB1* regulation of mammary basal cell fate and SC activity is currently lacking.

In this study, we used single-cell RNA sequencing (scRNA-seq) to survey the expression of EMT-associated genes in the adult MG epithelium and observed basal mammary epithelial cells (MECs) that show elevated *Zeb1* expression. Using epithelial-specific gene deletion and knockdown models, we provide unequivocal evidence that *Zeb1* is required within the mammary epithelium for ductal side branching and for the regenerative potential of basal SCs. Our findings demonstrate that *Zeb1* function is multi-faceted, as it governs basal-luminal balance by promoting basal cell fate and it acts within a population of quiescent G0 basal MECs to maintain their selfrenewal capacity. Furthermore, we identify Zeb1 as a direct transcriptional activator of *Axin2*, a feedback inhibitor of Wnt signaling. Finally, we show that inhibition of Wnt signaling in *Zeb1*-deficient basal MECs is able to partially rescue clonogenicity *ex vivo* and regeneration *in vivo*. Together, our study uncovers a previously unknown mechanism by which adult mammary basal cells utilize a core EMT-TF to coordinately maintain basal fate and SC quiescence.

RESULTS

Zeb1 expression in mammary basal MECs does not completely overlap with the expression of other EMT genes or known SC markers

To systematically probe EMT-associated gene expression heterogeneity in the mammary epithelium, we performed scRNA-seq analysis using the 10× Chromium platform on fluorescence-activated cell sorting (FACS)-isolated MECs from 8- to 9-week-old virgin females (Figure S1A). After filtering out low-quality cells and removing contaminating non-epithelial cell types (Figure S1B), we obtained a total of 15,580 MECs for downstream analysis. We observed five distinct epithelial clusters, including three (a basal cell cluster, an *Aldhla3*$^{+}$ luminal cell cluster, and a *Prlr/Esr1*$^{+}$ luminal cell cluster) that were previously described (Chung et al., 2019; Nguyen et al., 2018; Pal et al., 2017; Pervolarakis et al., 2020; Sun et al., 2018) and two small clusters of proliferative basal (*Acta2*, *Krt14*, *Topo2a*, and *Mki67*) or proliferative secretory luminal (*Csn3*, *Elf5*, *Topo2a*, and *Mki67*) cells (Figures 1A and S1C; Table S1). Importantly, cell clusters formed by basal MECs, but not luminal MECs, showed enrichment for an EMT-associated gene signature and for individual EMT-associated genes (e.g., *Vim* and *Snai2*; Figures 1B and S1D; Table S2). Enriched expression of EMT-associated genes (e.g., *Vim*, *Snai2*, and *Zeb1*) in basal MECs was further supported by our transcriptomic analysis of bulk MEC populations (Gu et al., 2013), which contrasted the enrichment of epithelial differentiation genes (e.g., *Cdh1*, *Ovol1*, and *Ovol2*) in bulk luminal cells (Figures 1C, S1E, and S1F; Table S3). qRT-PCR analysis of sorted basal, luminal, and stromal cells confirmed the inverse relationship between *Zeb1* and *Ovol2* expression, with basal cells showing intermediate levels of expression of these two genes (Figure 1D). Collectively, these data are consistent with mammary basal cells being in a transcriptional state that is intermediate between typical epithelial and mesenchymal states.

Next, we subset basal MECs from the combined 10× scRNA-seq data for further analysis. We also deep-sequenced full-length transcripts in 106 (86 of them passed quality control) FACS-isolated basal MECs using the Fluidigm C1 platform. Overall, *Vim* expression was detected in the largest fraction (86.2% in 10× and 68.9% in C1) of basal MECs, whereas other hallmark EMT-associated structural genes, such as *Cdh2* (2.9% in 10× and none in C1) and *Fn1* (3.3% in 10× and 51.5% in C1), were detected in fewer basal cells (Table S4). Among the EMT-TF genes, *Snai2* showed the most extensive basal MEC coverage (26.7% in 10× and 26.2% in C1), whereas *Zeb1* expression was detectable in 0.2% (10×) to 16.1% (C1) of basal MECs (Table S4). The low and variable frequencies of expression likely reflect the limited detection sensitivity of scRNA-seq, particularly for lowly expressed transcripts. Interestingly, the specific enrichment patterns of EMT-associated genes differ from each other and from those of known mammary SC markers, such as *Procr*, *Bcl11b*, *Cdh5*, *Lgr5*, *Tspan8*, and *Sox9* (Cai et al., 2017; Fu et al., 2017; Guo et al., 2012; Plaks et al., 2013; Sun et al., 2018; Wang et al., 2015; Figures 1E, 1F, and S1G; Table S5). Of note, *Procr* expression was enriched in basal MECs distinct from those showing high *Bcl11b* or *Axin2* expression (Figures 1E and 1F; Table S5), validating previously reported findings (Cai et al., 2017; Wang et al., 2015). Together, these data reveal previously unknown heterogeneity of EMT gene expression in the mammary basal compartment.

Next, we performed RNAScope experiments to co-analyze *Zeb1* expression with *Procr* or *Axin2* expression in the intact mammary tissue. As expected (Nassour et al., 2012; Wang et al., 2015; Ye et al., 2015), *Zeb1* transcripts were abundant in stromal cells surrounding the epithelial ducts of adult virgin MG (Figures 1G and 1H). However, we also detected *Zeb1* transcripts in 4%–9% of basal MECs and occasionally in luminal cells (Figures 1G–1J and S1H). The number of *Zeb1*-expressing basal MECs nearly doubled between 10 and 15 weeks of age (Figure 1J), a finding that was corroborated by qRT-PCR analysis, which revealed significantly elevated levels of *Zeb1* transcripts in basal MECs from 8 to 15 weeks of age in virgin mice (Figure 1K), as well as from virgin to mid-pregnant state (Figure S1I). *Procr* and *Axin2* transcripts were detected in ~3% and 40%–50%, respectively, of the basal MEC population (Figures 1G–1J). Of the *Zeb1*-expressing cells, more than half co-expressed *Axin2* and 15% co-expressed *Procr* (Figures 1I and 1J). We were unable to consistently detect *Zeb1* protein in basal MECs, likely due to weak and transient expression, but observed strong nuclear signals in the surrounding stroma (Figures S1J–S1L). Overall, our data demonstrate that *Zeb1* is weakly but dynamically expressed in basal MECs in a manner that shows partial overlap with known SC markers and that its expression is elevated as the mammary epithelium switches its major mode of morphogenesis from ductal elongation to side branching.

Zeb1 acts within basal MECs to promote mammary ductal side branching

To investigate *Zeb1* function specific to the mammary epithelium, we bred a floxed *Zeb1* allele (Brabletz et al., 2017) with *K14-Cre* (Kalailingam et al., 2017) mice to generate MEC-specific knockout (MSKO) of *Zeb1*. The *K14-Cre* line directed efficient and specific recombination in MECs, which was demonstrated by the robust GFP expression in mammary epithelium of *K14-Cre*;*mTmG* mice and the reduced level of *Zeb1* transcripts in FACS-sorted basal cells from *Zeb1* MSKO mice (Figures S2A–S2C). MGs from 6- to 8-week-old *Zeb1* MSKO females did not present any obvious morphologic defect and were able to undergo pregnancy-induced alveologenesis (Figures 2A, S2D, and S2E), which is consistent with previous finding that *MMTV-Cre*-driven *Zeb1* deletion does not affect pubertal mammary epithelial development (Fu et al., 2019). However, MGs from older (12–17 weeks of age) virgin *Zeb1* MSKO females showed significantly reduced branching complexity with lower numbers of secondary and tertiary branches compared with control littermates (Figures 2B and 2C). Reduced branching was also evident through histology, which revealed a significantly lower ductal density in MG sagittal sections of *Zeb1* MSKO mice (Figures 2D and 2E). Furthermore, when 12- to 17-week-old females were bred and analyzed at 14.5 days of pregnancy (P14.5), *Zeb1* MSKO MGs exhibited significantly reduced branching complexity compared to the controls (Figures 2F and 2G). Together, these data uncover a physiological role of *Zeb1* in the mammary epithelium to promote side branching in adult mice.

To ask whether *Zeb1* functions within the basal MEC population, we used recombinant lentiviruses that express GFP and distinct short hairpin RNAs (shRNAs) to effectively knockdown *Zeb1* expression in freshly isolated basal MECs from adult wild-type (WT) virgin females (Figures S2F–S2I) and subsequently transplanted the transduced cells into epithelia-cleared fat pads of syngeneic hosts. Compared with contralaterally transplanted

basal MECs that were transduced with lentiviruses expressing GFP and a scrambled sequence (shScr), *Zeb1*-depleted (sh*Zeb1*) basal MECs produced GFP^+ mammary trees with significantly fewer branching points (Figures 2H–2K and S2J–S2M). Collectively, results from these experiments provide convincing evidence that *Zeb1* functions within the mammary basal epithelial compartment to regulate ductal branching morphogenesis.

Zeb1 promotes basal cell fate and inhibits luminal cell fate through EMT-associated gene regulation

To ask whether *Zeb1* loss affects EMT-associated gene expression, we performed qRT-PCR analysis on FACS-isolated basal MECs. This analysis revealed significantly reduced expression of EMT/mesenchymal genes, including *Vim*, *Snai2*, *Cdh2*, and *Twist1*, but increased expression of epithelial gene *Cdh1* in *Zeb1* MSKO basal MECs compared with the control counterparts (Figure 3A). Therefore, *Zeb1* maintains basal MECs in a partial EMT-like transcriptional state.

Given the normally higher expression of EMT-associated genes in basal MECs than luminal MECs, we next asked whether *Zeb1* deletion affects basal-luminal balance. MECs cultured under conditions that induce differentiation are known to produce branched/solid and acinar-like organoids, which are derived from basal/stem and luminal/alveolar-restricted progenitor cells, respectively (Dontu et al., 2003; Gu et al., 2013; Jardé et al., 2016). We found that both lentivirus-mediated knockdown and adenovirus-Cre (Ade-Cre)-mediated knockout of *Zeb1* in MECs derived from WT and $Zeb1^{f/f}$ mice, respectively, resulted in a significant decrease in the ratio between branched/solid and acinar-like organoids, whereas the total number of organoids was not affected (Figures 3B, 3C, and S3A–S3E).

Next, we asked whether *Zeb1* influences fate determination *in vivo* by analyzing basal/luminal MEC ratio in *Zeb1* MSKO and control littermates using flow cytometry. No change in basal/luminal ratio was detected in MGs from 6- to 9-week-old *Zeb1* MSKO virgin females compared with control littermates (Figures S3F and S3G). However, we observed a significant decrease in basal/luminal ratio in MGs from 12- to 17-week-old *Zeb1* MSKO virgin females compared with control females (Figures 3D and S3H) and a trend of decrease in MGs from P14.5 pregnant *Zeb1* MSKO females (Figure S3I). We also immunostained *Zeb1* MSKO and control MGs for basal (K14) and luminal (K8) keratin markers. While $K14^+$ and $K8^+$ cells are well partitioned in the basal and luminal compartment, respectively, of the control MGs as expected, we detected ectopic K8 expression in $K14^+$ basal cells of the MSKO MGs (Figures 3E and S3J). Together, these findings show that *Zeb1* loss skews the balance between basal and luminal MECs towards the latter.

To determine whether *Zeb1* functions specifically within basal MECs to regulate lineage differentiation, we infected WT basal MECs with sh*Zeb1*- or shScr-expressing lentiviruses and subsequently cultured them under differentiating conditions to compare organoid morphology and expression of basal/luminal marker genes. Interestingly, while both sh*Zeb1* and shScr-expressing basal MECs produced organoids displaying a branched/solid morphology, the expression of transitional/luminal keratin marker *Krt19* (K19) (Pal et al., 2017) and luminal-fate-promoting gene *Notch1* (Bouras et al., 2008) was significantly elevated in *Zeb1*-depleted organoids (Figure 3F). However, the expression of *Krt14* (K14)

and *Krt8* (K8) was not affected (Figure 3F). Thus, *Zeb1* acts within the basal MEC population to maintain basal cell identity and prevent the acquisition of partial luminal features.

Next, we asked whether ZEB1/Zeb1 also regulates basal-luminal balance in MCF10A, a human MEC line that expresses both basal and luminal keratins (Keller et al., 2010; Neve et al., 2006; Qu et al., 2015; Sarrió et al., 2008). CRISPR-Cas9-mediated deletion of *ZEB1* led to increased expression of *KRT19* and decreased expression of *KRT14*, whereas the expression of *KRT8* was not significantly affected (Figure 3G). Conversely, treatment with transforming growth factor β (TGF-β), a well-known EMT/ZEB1-inducing factor (Xu et al., 2009), resulted in reduced *KRT19* expression and elevated *KRT14* expression without affecting *KRT8* expression (Figure 3G). In *ZEB1*-deficient cells, however, TGF-β not only induced *KRT19* down-regulation and *KRT14* upregulation but also significantly increased expression of *KRT8* (Figure 3G). These data underscore a tight association between EMT-associated molecular regulation and basal MEC fate and establish *ZEB1*'s role in promoting basal while suppressing luminal gene expression. Further supporting these conclusions, inducible overexpression of *Zeb1* in MCF10A cells led to a rapid increase in *KRT14* transcripts and decrease in *KRT19* transcripts, as well as a gradual expansion and reduction of cells that express K14 and K8 proteins, respectively (Figures 3H and S3J–S3M). Moreover, constitutive overexpression of *Zeb1* in MCF10A cells resulted in significantly enriched expression of both EMT/mesenchymal genes and a mammary basal SC gene signature (Lim et al., 2010), as revealed by RNA-seq analysis (Figure 3I). Therefore, *Zeb1*'s role in governing basal-luminal balance is likely conserved between mouse and human.

Our previous *in vitro* studies suggest a model where Zeb1 forms a direct cross-repression regulatory circuit with EMT-inhibiting TF Ovol2 to produce intermediate cellular states along the EMT spectrum (Hong et al., 2015; Lee et al., 2014). Although more highly expressed in luminal cells (Figures 1C and 1D), *Ovol2* transcripts were also detected in a small number of basal cells that do not show enrichment for *Zeb1* (Figure 1E). To determine whether a *Zeb1*-Ovol2 circuit operates within MECs to regulate basal/luminal cell fate, we conducted two lines of experiments. First, we performed qRT-PCR on sorted basal MECs to find that *Zeb1*-deficient cells showed increased expression of *Ovol2*, whereas *Ovol2*-deficient cells showed increased expression of *Zeb1* (Figures 3J and S3N). Second, we applied the Ade-Cre deletion system to MECs derived from compound mutant mice containing floxed *Zeb1* and *Ovol2* alleles (Figures 3K, S3O, and S3P) to ask how acute deletion of *Zeb1* and/or *Ovol2* affects basal-luminal balance. Opposite to the effects of *Zeb1* deletion alone ($Zeb1^{f/f}Ovol2^{f/+}$) and compared with the $Zeb1^{f/+}Ovol2^{f/+}$ control, deletion of *Ovol2* alone ($Zeb1^{f/+}Ovol2^{f/f}$) led to an increased ratio between branched (basal-type) and acinar (luminal-type) organoids (Figure 3L). Remarkably, simultaneous deletion of both genes (double knockout [DKO], $Zeb1^{f/f}$Ovol2$^{f/f}$) restored the branched/acinar organoid ratio to control levels (Figure 3L). This said, a significant fraction of the DKO organoids exhibited atypical morphology (Figure S3Q), suggesting that each gene also performs a unique function. Together, these results indicate that *Zeb1*'s role in promoting basal fate and inhibiting luminal differentiation is in part mediated through EMT-associated gene regulation.

Zeb1 is required for maximal regenerative potential and clonogenicity of basal MECs

To directly assess whether *Zeb1* regulates basal SC activity, we performed limiting dilution transplantation experiments using GFP^+ control and *Zeb1* knockdown basal MECs to estimate the frequency of mammary repopulating units. We found *Zeb1* depletion to significantly reduce the take rate at all dilutions tested (Figures 4A and S4A). We also transplanted the GFP^+ subset of Ade-Cre-infected basal MECs isolated from $Zeb1^{f/+}$ and $Zeb1^{f/f}$ mice and analyzed the resulting fat pad outgrowths. Compared with $Zeb1^{f/+}$ cells that were able to generate a complete epithelial network, $Zeb1^{f/f}$ (*Zeb1* KO) cells either failed to produce any mammary tree or produced only a rudimentary tree (Figures 4B and S4B). Moreover, we transplanted *Zeb1* KO basal MECs along with *Zeb1*/*Ovol2* DKO basal MECs and observed a partial rescue in mammary tree regeneration in the latter (Figure S4C). Finally, we transplanted basal MECs isolated from MGs of 8- to 9-week-old *Zeb1* MSKO and control littermate mice and found MSKO cells to produce either none or truncated trees (Figure 4C). Therefore, *Zeb1*-deficient basal MECs are already inherently defective at this early stage, which can be unraveled by the SC-demanding regenerative assay (Van Amerongen et al., 2012).

To complement the *in vivo* findings above, we cultured basal MECs derived from 8-week-old *Zeb1* MSKO mice and their control littermates under proliferative conditions to compare clonogenicity. *Zeb1* MSKO basal MECs were initially able to form colonies, and the number of colonies formed was even higher than the control cells (Figures 4D and S4D). However, with passaging, both the number and size of the colonies produced by *Zeb1*-deficient basal MECs became significantly smaller than the controls (Figures 4D and S4D). We also analyzed basal MEC colonies derived from 15-week-old *Zeb1* MSKO mice and control littermates and found that the *Zeb1*-deficient colonies not only are smaller than their control counterparts but also show ectopic K19 expression in the outer $K14^+$ compartment (Figure S4E). These data are consistent with stem/progenitor cell exhaustion and precocious luminal differentiation as a result of *Zeb1* loss.

Collectively, our results from three independent genetic approaches (acute basal-specific knockdown, acute basal-specific KO, and MEC-specific KO) yield the same conclusion that *Zeb1* is required within the mammary epithelium (basal MECs in particular) for optimal mammary epithelial tissue regeneration and SC maintenance.

Zeb1 maintains a quiescent population of basal MECs and preserves their self-renewal

To probe deeper into the cellular mechanism by which *Zeb1* functions in basal MECs, we analyzed the cell cycle profile of MECs in *Zeb1* MSKO and control mice using a method that quantifies RNA and DNA contents in cell populations through flow cytometry (Eddaoudi et al., 2018; Kim and Sederstrom, 2015). At 8 to 9 weeks of age, *Zeb1* MSKO basal MEC population showed an ~7-fold reduction in cells at G0 and ~2-fold increase in cells at G2/M phases of the cell cycle compared with their control counterparts, whereas the number of cells at G1 and S phases was similar (Figures 5A and 5B). In addition, Ki67 staining revealed a significant increase in the number of proliferative basal MECs in *Zeb1* MSKO mice compared with control counterparts, whereas the number of $Ki67^+$ luminal cells was unaffected (Figures 5C and 5D). Together, these data suggest that *Zeb1*

deletion results in an early burst of basal MEC proliferation, a conclusion further supported by a significantly higher number of basal MECs in 8- to 9-week-old *Zeb1* MSKO MGs compared with control counterparts (Figures 5E and S5A). Comparatively, at 12 weeks of age, fewer *Zeb1* MSKO basal MECs resided in G0 or S/G2/M, whereas more resided in G1 than controls (Figures 5F and 5G). In contrast, *Zeb1* MSKO luminal cells did not exhibit significant cell cycle differences at either young (8- to 9week) or older (12-week) ages when compared with controls (Figures S5B–S5E). The overall picture emerging from the temporal analyses is that *Zeb1*-deficient basal MECs are less able to maintain a quiescent G0 state in the adult MG, which results in an initial increase in cell division that is followed by eventual depletion of proliferative basal MECs.

Next, we assessed whether *Zeb1* acts within the G0-phase basal MECs to regulate their ability to self-renew. We first FACS-sorted G0 and G1 basal MECs from adult WT mice and compared their capacity to form colonies *ex vivo*. Importantly, G0 basal MECs formed significantly more colonies than their G1 counterparts (Figures 5H and S5F), which is consistent with the stem/progenitor cell nature of these cells. We then infected G0 and G1 basal MECs with shScr- or sh*Zeb1*-expressing lentiviruses to deplete *Zeb1* (Figure S5G) and analyzed colony formation. The number of colonies produced by G0 cells was significantly reduced upon *Zeb1* depletion, while the average colony size was not affected (Figures 5I and S5H). In contrast, neither the number nor the size of colonies produced by G1 cells was affected by *Zeb1* depletion (Figures 5I and S5H). These data identify a specific role of *Zeb1* in promoting G0 basal MEC clonogenicity.

Next, we performed bulk RNA-seq analysis on sorted G0 and G1 basal MECs and identified a G0-enriched 21-gene signature that included *Cdh5*, a known marker of quiescent basal MECs (Sun et al., 2018), and genes previously shown to be upregulated in the highly quiescent *Lgr5*$^{+}$ *Tspan8*^{high} basal SCs (*Thbd*, *Lrrc32*, *Cd36*, and *Nrp1*) or required for mammary development and basal SC activity (*Nrp1*; Fu et al., 2017; Liu et al., 2017; Figure S5I; Table S7). Proof-of-principle qRT-PCR analysis validated the elevated expression of several genes within this signature (e.g., *Cdh5*, *Nrp1*, *Rnf125*, *Ushbp1*, and *Cd3001g*) in independently sorted G0 basal MECs over G1 basal MECs (Figure S5J). Although not identified as part of the 21-gene signature, *Zeb1*, *Vim*, and known basal quiescence marker *Bcl11b* were found using qRT-PCR analysis to be expressed at higher levels in G0 basal MECs than in G1 basal MECs, whereas expression differences of other EMT genes were variable (Figures 5J, S5J, and S5K). Importantly, the transcript levels of all G0-enriched genes tested (*Cdh5*, *Nrp1*, *Rnf125*, *Ushbp1*, *Cd3001g*, and *Bcl11b*) were significantly reduced in *Zeb1* MSKO basal MECs compared with the control counterparts (Figure 5K). Taken together, our findings suggest that *Zeb1* functions within the quiescent G0 basal MEC population to preserve their proliferative potential and unique gene expression.

Zeb1 inhibition of Wnt signaling is important for mammary basal SC self-renewal

Our finding that *Ovol2* deletion does not fully rescue the regenerative and differentiation potential of *Zeb1* KO basal MECs implicates additional molecular mechanisms underlying *Zeb1*'s function. Given the well-known role of Wnt signaling in mammary side branching and basal SC self-renewal (Alexander et al., 2012; Van Amerongen et al., 2012; Brisken et

al., 2000; Fu et al., 2020; Gu et al., 2013; Liu et al., 2005; Watanabe et al., 2014; Woodward et al., 2005; Zeng and Nusse, 2010), we wondered whether there is a possible connection between *Zeb1* and Wnt signaling. Interrogating a publicly available ZEB1 chromatin immunoprecipitation sequencing (ChIP-seq) dataset (University of California, Santa Cruz [UCSC] Genome Browser), we found ZEB1-binding peaks in an annotated enhancer region upstream of *AXIN2*, a direct target and feedback inhibitor of Wnt signaling (Behrens et al., 1998; Jho et al., 2002; Zeng and Nusse, 2010; Figure S6A). Although ChIP-PCR on FACS-sorted basal MECs was unsuccessful, likely due to low or rare *Zeb1* expression, specific binding of ZEB1 to E-box recognition motifs in the *AXIN2* enhancer was detected in MDA-MB-231 human breast cancer cells, which are well documented for their high EMT gene expression (Watanabe et al., 2014; Figure 6A). Moreover, qRT-PCR analysis revealed reduced *Axin2* expression in both *Zeb1*-depleted basal MEC-derived colonies and in freshly FACS-sorted basal MECs from *Zeb1* MSKO mice compared with control counterparts (Figures 6B and 6C). Consistent with the inverse relationship between *Axin2* and Wnt signaling output, multiple downstream target genes of Wnt signaling, including *Lef-1*, *c-Myc*, *Tfrc*, and *LBH* (He et al., 1998; Hovanes et al., 2001; Lindley et al., 2015; Röhrs et al., 2009), showed significantly increased expression, whereas *Plf1* and *Ramp3*—genes known to be repressed by Wnt signaling (Röhrs et al., 2009)—showed decreased expression in *Zeb1* MSKO basal MECs compared with control counterparts (Figure 6C).

Zeb1 is well known for its function as a transcriptional repressor but can also activate transcription when complexed with YAP (Feldker et al., 2020; Lehmann et al., 2016). Strong and widespread presence of nuclear YAP protein in basal MECs of adult virgin MGs has been reported (Chen et al., 2014). In ChIP-PCR assays using MDA-MB-231 cells, we found YAP protein to bind to the *AXIN2* gene at the same sites occupied by ZEB1 (Figure 6A). Moreover, *Zeb1* overexpression in MCF10A cells led to enriched expression of a YAP gene signature (Figure S6B). To determine whether *Zeb1* is able to activate *AXIN2* enhancer activity, we cloned an *AXIN2* DNA fragment containing the ZEB1/YAP binding sites into a PGL3-promoter vector and co-transfected the resulting luciferase construct into 293T cells with Zeb1- and/or YAP-expressing constructs. While exogenous Zeb1 or YAP alone induced minimal to no luciferase reporter activity, significant luciferase activity was observed when Zeb1 and YAP were introduced together (Figure 6D). Moreover, site-directed mutagenesis of two E-box motifs in the *AXIN2* enhancer abolished the Zeb1/YAP-dependent activation (Figure 6E). Together, these findings suggest a molecular model where Zeb1 functions cooperatively with YAP to directly activate the expression of *Axin2*.

Despite the well-established role of canonical Wnt signaling in promoting mammary basal SC self-renewal and expansion, our findings of downregulated expression of Wnt inhibitor *Axin2* and elevated expression of Wnt target genes in *Zeb1*'s absence raise the possibility that excessive Wnt signaling may be detrimental to basal SC maintenance. To address this, we first asked whether the effect of Wnt signaling on basal MEC expansion is dosage dependent. While addition of recombinant Wnt3a at a low concentration stimulated colony formation by basal MECs, Wnt3a addition at a high concentration significantly impaired colony formation to an extent similar to the inhibition observed after the addition of 6-bromoindirubin-3'-oxime (BIO), a small molecule that stimulates Wnt signaling through inhibition of glycogen synthase kinase-3 (Meijer et al., 2003; Figures 7A and S7A). qRT-

PCR analysis confirmed the elevated expression of Wnt target genes *Lef-1* and *c-Myc* following *Wnt3a* addition (Figure 7B).

Next, we asked whether inhibition of Wnt signaling by exogenous application of extracellular inhibitor Dkk1 (Glinka et al., 1998) rescues the colony formation defects observed in *Zeb1* MSKO basal MECs. We found recombinant Dkk1 to severely impair colony formation (both number and size) in basal MECs that were isolated from either 8- or 15-week-old control females (Figures 7C and 7D), reinforcing the expected dependence of normal basal MEC proliferation on Wnt signaling. Interestingly, however, basal MECs isolated from 8-week-old *Zeb1* MSKO mice were refractory to Dkk1 inhibition (Figure 7C). Moreover, Dkk1 treatment of basal MECs from 15-week-old *Zeb1* MSKO mice led to a significant improvement in colony formation (Figure 7D). The expression of *Lef-1* and *c-Myc* was decreased by Dkk1 as expected, and the expression levels in *Zeb1*-deficient cells were restored to near-control levels (Figure 7E).

We also examined whether Dkk1 treatment rescues the regenerative defect of *Zeb1*-deficient basal MECs. When *Zeb1* MSKO basal MECs from 15-week-old mice were pre-incubated with Dkk1-coated beads prior to being transplanted into epithelia-cleared fat pads, their ability to regenerate an epithelial ductal network was significantly improved compared with when BSA-coated control beads were used, whereas the regenerative potential of control basal MECs was reduced by pre-incubation with Dkk1 (Figures 7F, 7G, and S7B). Together, our data show that excessive Wnt signaling activity is in part responsible for the *Zeb1* deletion-induced decrease in basal MEC clonogenicity and regenerative potential.

DISCUSSION

Numerous studies have established that mammary basal MEC fate, but not luminal MEC fate, is compatible with stemness and remarkable “hidden” plasticity that can be unraveled when the cells are placed into a permissive microenvironment (e.g., upon transplantation). Compared with luminal epithelial cells and stromal mesenchymal cells, basal MECs co-express epithelial and mesenchymal genes and are in a transcriptional state that resembles the so-called intermediate or hybrid state within the EMT spectrum. Key but largely open questions include (1) are core EMT-TFs physiologically exploited to support basal-specific gene expression, thereby enabling or maintaining a basal MEC fate; (2) is maintaining a partial EMT-like transcriptional state functionally important for, and coordinately regulated with, the essential cellular activities of basal MECs, such as proliferation and quiescence; and (3) do core EMT-TFs acquire non-canonical functions to regulate unique aspects of mammary epithelial morphogenesis, SC function, and developmental signaling? Our study now provides a vigorous body of experiments to answer these important questions at both functional and mechanistic levels.

Our work has identified *Zeb1* as an epithelial-intrinsic and physiological regulator of mammary side branching morphogenesis. We show that an important and conserved aspect of *Zeb1* function is to promote basal cell fate and suppress luminal differentiation, and this role is likely linked to its ability to maintain the basal MECs in a partial EMT-like transcriptional state (Figure 7H). *Zeb1* regulation of basal-luminal balance is somewhat

reminiscent of the role of *Snai2*, which when deleted in the germline causes increased mammary luminal gene expression (Nassour et al., 2012) and when ectopically expressed in conjunction with Sox9 can turn luminal cells into basal-like SCs (Guo et al., 2012). Although the expression patterns and deletion phenotypes of *Zeb1* and *Snai2* in the MG are distinct, an emerging common theme is that robust maintenance of mammary basal cell fate requires the function of core EMT-TFs.

The major ductal expansion events that occur during pubertal development to fill the mammary fat pad are driven by the highly proliferative terminal end buds—located at the tips of growing ducts—that apparently lack quiescent SCs (Fu et al., 2017). As the MG transitions into homeostasis, the mode of morphogenesis switches from massive tissue expansion to cyclic bouts of growth and regression that occur with each estrus cycle and that become dramatically elaborated during the reproductive cycle of pregnancy, lactation, and involution. Interestingly, this transition is accompanied by doubling the G0/G1 basal MEC ratio from 14.3%/69.8% at 8 to 9 weeks to 20.5%/47.5% at 12 weeks of age (Figures 5B and 5G). Known regulators of quiescent basal SCs include *Bcl11b*, which suppresses G1 cell cycle progression, and *Foxp1*, which promotes *Tspan8*^{high} stem cell exit from quiescence (Cai et al., 2017; Fu et al., 2018). Distinct from *Bcl11b* or *Foxp1*, the deletion of which arrests pubertal ductal expansion, *Zeb1* loss results in defective side branching in adulthood and a transient burst of basal cell division followed by eventual exhaustion of proliferation potential. Therefore, we surmise that *Bcl11b* and *Zeb1* promote the quiescence of two distinct (albeit not necessarily mutually exclusive) populations of basal SCs, those that sustain estrogen/amphiregulin-driven pubertal development versus those that fuel progesterone/Wnt4/Rankl-driven side branching and long-term regeneration in adulthood (Arendt and Kuperwasser, 2015; Ciarloni et al., 2007; Fu et al., 2020; Sternlicht et al., 2006). As such, our study identifies, for the first time, a critical regulator of adult mammary epithelial basal SC quiescence.

Precedents for dosage-, context-, and stage-specific effects of Wnt signaling have been described for SCs in the hair follicle and hematopoietic lineages (Lowry et al., 2005; Richter et al., 2017). Spatiotemporal control and dose-dependent role of Wnt signaling in mammary SCs have also been implicated by previous studies; for example, the most quiescent basal SCs express high levels of Wnt signaling inhibitors, such as *Sfrp* genes (Fu et al., 2017; Macias et al., 2011; Roarty et al., 2015). Our study now provides the first definitive evidence that maintaining a low level of Wnt signaling output is functionally required for adult basal SC maintenance and that a core EMT-TF (*Zeb1*) is required to keep Wnt signaling activity in check in order to preserve basal SCs (Figure 7H).

Although our qRT-PCR analysis revealed altered expression of EMT-associated, G0-enriched, or Wnt target genes in basal MECs upon *Zeb1* deletion, RNA-seq and assay for transposase-accessible chromatin with high-throughput sequencing (ATAC-seq) analyses of basal MECs failed to reveal robust and statistically significant differences between control and *Zeb1* MSKO samples (unpublished data). This may not be surprising, given the small number of cells showing detectable *Zeb1* expression. We envision that *Zeb1* expression might be activated in a small fraction of basal MECs when they enter or pass a fluidic cellular state, but it may yield long-lasting impact even after expression is turned off. In

addition, *Zeb1* may regulate the expression of secreted molecules that exert paracrine effects on other basal MECs. We note the interesting recent discovery that *Zeb1*-expressing cells in the prostate represent multipotent basal SCs with self-renewal potential (Wang et al., 2020). The availability of genetic tools to track and manipulate *Zeb1*-expressing cells *in situ* (Wang et al., 2020) combined with the advent of high-order MG imaging technology (Fu et al., 2017; Rios et al., 2014) will enable future investigation into whether *Zeb1*-expressing basal MECs are a SC subset in adult MG.

In summary, our findings underscore both EMT-dependent and -independent functions of *Zeb1* in governing mammary basal cell fate and adult SC maintenance. The insights gained not only expand our knowledge of tissue SC control but also shed new light onto the complex effects of core EMT-TFs on tumorigenesis and cancer cell stemness (Brabletz and Brabletz, 2010).

Limitations of the study

Our study is limited by the lack of *in vivo* data to show cooperative function of Zeb1 and YAP in adult MG and the lack of functional data to definitively show that Zeb1 inhibits Wnt signaling through expression of *Axin2*. Future studies are needed to address these deficiencies.

STAR★METHODS

RESOURCE AVAILABILITY

Lead contact—Further information and requests for resources and reagents should be directed to, and will be fulfilled by, the Lead Contact, Xing Dai (xdai@uci.edu).

Materials availability—This study did not generate new unique reagents.

Data and code availability—The scRNA-seq and bulk RNA-seq data reported in this work have been deposited in the GEO database under accession numbers GEO: GSE155636, GEO:GSE70551, and GEO: GSE188781. This paper does not report original code. Any additional information required to reanalyze the data reported in this paper is available from the lead contact upon request.

EXPERIMENTAL MODEL AND SUBJECT DETAILS

The floxed alleles of *Zeb1* and *Ovol2* were as described (Brabletz et al., 2017; Unezaki et al., 2007). The *K14-Cre* [B6N.Cg-Tg(KRT14-cre)1Amc/J, Stock # 018964] and *mTmG* [Gt(ROSA)26Sortm4(ACTB-tdTomato,-EGFP)Luo, Stock # 007676] mice were purchased from the Jackson Laboratory. Genotyping was performed using PCR primers (Table S6) as previously described (Andl et al., 2004; Brabletz et al., 2017; Unezaki et al., 2007) or per company specifications. Female mice were used for analyses, at the ages indicated in the relevant Figure Legends. All mouse lines were maintained in a specific pathogen-free facility, following mouse procedures that conform and have been approved by the University of California Irvine Institutional Animal Care and Use Committee.

METHOD DETAILS

Mammary cell preparation, flow cytometry, and FACS—Preparation of single mammary cells suspensions and the procedures for flow cytometry analysis or fluorescence-activated cell sorting (FACS) were performed as previously described (Gu et al., 2009, 2013; Watanabe et al., 2014). Briefly, MGs were isolated from mice and dissociated by incubating with 300 U/mL collagenase (Sigma, C9891) and 100 U/mL hyaluronidase (Sigma, H3506) for 1.5 hours at 37°C. After vortexing and lysis using the red blood cells lysis buffer (Sigma, R7757), a single-cell suspension was obtained by sequential dissociation of the fragments by gentle pipetting for 2 min in 0.25% trypsin (Gibco, 25200), and then for 2 min in 5 mg/ml dispase II (Stem Cell Technologies, 07913) plus 0.1 mg/ml DNase I (Sigma, DN25), followed by filtration through a 40 μm mesh (SWiSH, TC70-MT-1). For all mammary cell isolations, viable cells were counted on a hemacytometer using trypan blue exclusion.

For flow analysis and basal MEC ($Lin^{-}CD49f^{high}EpCAM^{+}$) sorting, cell pellets from the single-cell suspensions were resuspended in 2% FBS in PBS, and then stained at room temperature for 30 minutes in a 500 μL mix containing the following cell-surface marker antibodies: allophycocyanin (APC)-labeled lineage antibodies [including CD45 (BD Biosciences, 559864), CD31 (BD Biosciences, 551262), and TER119 (BD Biosciences, 557909)], phycoerythrin (PE)/Cy7-labeled CD326 (EpCAM) (Bio Legend, 118215), and fluorescein isothiocyanate (FITC)-labeled CD49f (Bio Legend, 555735).

For analysis and sorting of G0 and G1 basal MECs, MG cell pellets were first stained with cell-surface markers as described above, washed once with FACs buffer (PBS with 2% FBS), followed by staining with 10 μg/ml Hoechst 33342 (Life technology, H3570) and 1 μg/ml Pyronin Y (Santa Cruz, 92–32-0) for 30 min at 37°C in the dark. The cells were then rinsed with FACS buffer and immediately analyzed on Novocyte (ACEA Biosciences Inc) using the Pacific Blue channel for Hoechst and PE channel for Pyronin Y. Control and *Zeb1* MSKO littermates housed in the same cages were used for this analysis, and the cell cycle differences observed were not due to estrus cycle differences based on PCR analysis of their uterus RNAs (data not shown). Live-cell sorting was performed on an FACSAria cell sorter (Becton Dickenson UK) equipped with FACS DiVa6.0 software operating at low pressure (20 psi) using a 100 μm nozzle. Cell clusters and doublets were electronically gated out. Cells were routinely double sorted, and postsort analysis typically indicated purities of >90% with minimal cell death (<10%).

scRNA-seq analysis—For scRNA-seq using the 10X Chromium system, FACS-sorted mammary basal and luminal cell populations were combined. Library generation and Illumina HiSeq-4000 sequencing were performed as previously described (Haensel et al., 2020). For scRNA-seq using the Fluidigm C1 platform, FACS-sorted basal MECs ($Lin^{-}CD49f^{high}EpCAM^{+}$) were washed and resuspended with Epicult-B medium (Stem Cell Technologies; Ca. No. 05610) at a concentration of ~500 cells/μL. Cell suspensions were mixed with Fluidigm C1 Suspension Reagents (Fluidigm 100–5315) at a ratio of 8:2 before loading onto the C1 chip (Fluidigm 100–5760). Bright-field images of captured cells were collected using a Keyence BZ-X710 microscope (Keyence Corporation, Itasca, Illinois, USA). Single-cell RNA isolation and amplification were performed using the Fluidigm C1

Single Cell Auto Prep IFC following the Fluidigm Protocol #100–7168 I1. RNA spike-in controls were omitted. cDNA library preparation was performed following the Fluidigm C1 Protocol #100–7168 I1.

Data analysis was performed using Seurat as we previously described (Haensel et al., 2020). Heatmaps were based on normalized, but not raw, values of expression to enable direct comparison across runs. A color gradient depicting the expression of each gene in each cell per average for all the cells was generated for each analysis combining biological replicates.

Morphological, histological, and immunostaining analyses—Whole-mount analysis and H/E staining of dissected MGs were as previously described (Watanabe et al., 2014). Indirect immunofluorescence was performed as described (Lee et al., 2014) using the following antibodies: Zeb1 (Rabbit; 1:250, Novus Biologicals, NBP1-88845; 1:100, Santa Cruz, sc-25388), Ki67 (1:1000, Cell Signaling, 9129), SMA (Rabbit; 1:500, Abcam, ab5694), K14 (Chicken; 1:500, a gift from J. Segre, National Institutes of Health, Bethesda, MD), or K8 (Rat; 1:500, Developmental Hybridoma, TROMA-I). The following secondary antibodies were used: goat anti-rabbit IgG (H+L) cross-absorbed secondary, Alexa Fluor-488 (1:500, Life technologies, A11008) or rhodamine red-X (RRX) Affini-pure goat anti-chicken IgY (IgG) (H+L) (1:500, Jackson Immunoresearch, 103–295-155).

RNAScope, RT-qPCR, and bulk RNA-seq—RNAScope was performed as previously described (Haensel et al., 2020), except that 10-μM MG OCT sections were fixed in 4% paraformaldehyde for 1 hour at room temperature. The following probes were used: *Zeb1* (ACD; 451201-C1), *Procr* (ACD; 410321-C2), and *Axin2* (ACD; 400331-C2). Anti-K14 antibody was used to stain the basal MECs. The images were acquired with a Zeiss LSM 700 confocal microscope, and ZEN 2010 software was used to manually count the number of signal-positive and basal MECs.

For RT-qPCR, cDNA was prepared using High-Capacity cDNA Reverse Transcription Kit (Thermo Fisher Scientific) according to manufacturer's instructions. Real-time PCR was performed using a CFX96 RT-qPCR system and SYBR Green Supermix (BioRad). Comparative analysis using delta-delta Ct method was performed between the gene of interest and the housekeeping gene *Gapdh*/*GAPDH*. Sequences of primers used to analyze gene expression are described in Table S7.

For bulk RNA-seq analysis, G0 and G1 cells were sorted into RNA lysis buffer (R1050, Zymo Research), and RNAs were isolated and purified using Quick-RNA Microprep (R1050, Zymo Research) per manufacturer's protocol. RNAs were quantified using the NanoDrop ND-1000 spectrophotometer (ThermoFisher) and quality checked using the Agilent Bioanalyzer 2100 (Agilent). Library construction was performed according to the Illumina TruSeq® Stranded mRNA Sample Preparation Guide. One μg of total RNA was used and mRNA was enriched using oligo dT magnetic beads. The enriched mRNA was chemically fragmented for 3 min, followed by reverse transcription to make cDNA. The resulting cDNA was cleaned using AMPure XP beads, end repaired, and the 3' ends were adenylated. Illumina barcoded adapters were ligated on the ends and the adapter-ligated fragments were enriched by 9 PCR cycles. The resulting libraries were validated by qPCR

and sized by Agilent Bioanalyzer DNA High Sensitivity Chip. The barcoded cDNA libraries were multiplexed on the Illumina HiSeq 4000 platform to yield 100-bp paired-end reads. FASTQ files were trimmed using Trimmomatic version 0.35 (Bolger et al., 2014) and aligned to the mm10 genome and counted using STAR version 2.5.2a (Dobin et al., 2013). Differential expression analysis was performed using DESeq2 version 1.24.0 (Love et al., 2014) on R version 3.6.1. Differentially expressed genes were defined by having and adjusted p value < 0.05.

Transplantation assays—Transplantation of MECs into cleared fat pads of C57BL/6 mice were as previously described (Watanabe et al., 2014). Typically, 2000 FACS-sorted basal MECs or 5000 unsorted MECs were used for each transplantation unless otherwise indicated. Lentiviral infection before transplantation and *Zeb1* shRNA-expressing lentiviruses were as described previously (Watanabe et al., 2014). For limiting-dilution transplantation, GFP^+ cells were FACS-sorted following lentivirus infection and then transplanted into cleared fat pads.

For basal MEC transplantation with Dkk1-coated beads, Affi-Gel blue beads (Bio-Rad Laboratories, 1537301) were washed three times with PBS and incubated with 1 mg/ml recombinant mouse Dkk1 (R&D Systems, 5897-DK-010) in 0.1% BSA for 1 hour before transplantation. Approximately 100 beads were then mixed with 2000 FACS-sorted basal MECs in 10 μL of DMEM/F-12 medium containing 5% FBS, which were injected into cleared fat pads. Beads coated with 0.1% BSA were used as a control.

Colony and organoid formation assays—For colony formation, single cell suspensions of unsorted MECs or FACS-sorted basal MECs were embedded in 100% chilledgrowth factor-reduced Matrigel (BD Biosciences, CB-40230) and plated onto 8-well chamber slides at a density of 2×10^4 cells (unsorted MECs) or 5×10^3 (sorted basal MECs) per 50 μL Matrigel per well. After the Matrigel is set, the gel was covered with 400 μL EpiCult-B medium (Stem Cell Technologies, 05610) containing 10 ng/mL EGF (Millipore, 01–107), 10 ng/mL FGF-2 (PeproTech, 100–18B), and 4 μg/mL heparin (Stem Cell Technologies, 07980). The medium was replaced every 3 days, and colonies were analyzed at 14 days after plating. When appropriate, recombinant Wnt3a (R&D, 5306-WN), BIO (Millipore Sigma, B1686), or Dkk1 (R&D, 5897-DK) was added at the 1^{st} day of culture.

For passaging, Matrigel in each well (50 μL) was dissolved with Dispase (200 μL of 5 U/ml). Following a PBS wash, 200 uL of. 0.25% trypsin was added to dissociate cells for 5 min at 37°C. Reaction was then stopped by adding 1 mL of the culture medium. Cells were rinsed with 5% FBS in DMEM/F-12, counted, and plated at 5000 cells per well.

For organoid formation, EpiCult-B medium from above was removed after a week in culture and replaced with a DMEM/F12 Basal Medium (Invitrogen, 12500–062) containing 1% fetal bovine serum (FBS) (Omega Scientific, FB-02), 5 mg/mL insulin (Sigma, 16634), 500 ng/mL hydrocortisone (Calbiochem, 386698), and 5 mg/ml prolactin (Sigma, L6520) to induce differentiation. Three weeks later, organoids were fixed with 4% paraformaldehyde for analysis.

For RT-qPCR of colonies/organoids, 200 μL Dispase (5 U/ml) was added to each well to dissolve the Matrigel, followed by one wash in PBS. Then 200 μL of 0.25% trypsin was added to dissociate the colonies at 37°C until they became single cells, at which time the reaction was stopped by adding 1 ml of DMEM/F12 medium. Cells were then washed with PBS and resuspended in 300 μL of RNA lysis buffer (R1050, Zymo Research).

shRNA-mediated knockdown—The efficacy of shRNAs against *Zeb1* was tested using 3T3 mouse fibroblasts. To detect Zeb1 protein, nuclear extracts were isolated and Western blot analysis performed as previously described (Wells et al., 2009). Knockdown in MECs was performed as previously described (Watanabe et al., 2014).

Ade-Cre-mediated gene deletion—Ade-Cre were purchased from Vector Biolabs. MECs or FACS-sorted basal MECs were plated at 10 million/mL/well in 24-well plates in DMEM/F12 (Stemcell Technologies, 36254) containing 2% FBS, 10 mM HEPES (Millipore Sigma, H3375), 10 ng/ml EGF (Invitrogen, PMG-8043), 250 ng/ml Rspo1 (R&D, 3474-RS), 100 ng/ml Noggin (Fisher Scientific, 50–399-006), and 10 μM Rock inhibitor Y27632 (Millipore Sigma, SCM075), and cultured overnight. Cells were then infected with Ade-Cre at a multiplicity of infection (MOI) of 10 for overnight in 24-well ultra-low attachment surface polystyrene plate (Corning, REF 3473). Cells were harvested the next day, and treated with 400 μL TrypLE Select (GIBCO, 12605–010) for 20 min at 37°C followed by neutralization with 2 mL HBSS buffer (GIBCO, 14025134). GFP^+ cells were FACS-sorted for *ex vivo* culture or for transplantation.

***ZEB1* deletion and overexpression in MCF10A cells—**MCF-10A cell lines with CRISPR/Cas9-mediated *ZEB1* knockout or inducible Zeb1 overexpression were described in a previous study (Watanabe et al., 2014). For constitutive overexpression of Zeb1, recombinant lentiviruses were generated using pHIV-Zsgreen lentiviral constructs (Welm et al., 2008) and cloned mouse *Zeb1* cDNA. Production and infection of lentiviruses were carried out as previously described (Watanabe et al., 2014).

ChIP-PCR—MDA-MB-231 cells were cultured in 150-mm dishes as previously described (Watanabe et al., 2014). ChIP was performed as previously described (Gu et al., 2013) with modifications. Briefly, cells were cross-linked with 1% formaldehyde for 10 minutes at room temperature, followed by quenching with 0.125 M glycine for 5 minutes at room temperature. After washing, chromatin was sheared to produce ~100–500-bp fragments using Bioruptor Sonicator (Diagenode Inc.) at “high” setting with 30-second ON and 30-second OFF cycles for a total of 30 minutes. A small aliquot of the recovered supernatant underwent subsequent reverse crosslinking and DNA purification, and the resulting DNA was used to assess concentration and shearing efficiency (input sample). Twenty-five μg of the crosslinked chromatin in the remaining supernatant was immunoprecipitated by overnight incubation at 4°C with control IgG (Santa Cruz Biotechnology, sc-2027) or anti-ZEB1 (Novus Biologicals, NBPI-88845), anti-ZEB1 (Santa Cruz Biotechnology, h-102), or anti-YAP1 (Cell Signaling Technology, 8418) antibodies. Antibody-chromatin immunocomplexes were then purified as previously described (Gu et al., 2013). ChIP DNA

was recovered and purified using phenol: chloroform: isoamyl alcohol purification and then used for real-time PCR using primers listed in Table S6.

Molecular cloning and luciferase assays—A 2810-bp upstream region from the *AXIN2* gene (−3576 bp to −766 bp) was cloned into the PGL3-promoter construct (Addgene, E1760) using primers listed in Table S6. Deletion construct was generated by site-directed mutagenesis (Biolabs, E0554S) using primers listed in Table S6, and was sequence verified. The promoter constructs (0.5 μg) were transfected into 293T cells (1 well in 12-well plates) together with 1 μg of Zeb1- and/or YAP-expressing constructs and 100 ng of β-actin-β-galactosidase construct (transfection control). pCB6+ (empty vector containing the cytomegalovirus promoter) was used as filler DNA. The cells were harvested two days after transfection, and luciferase activity was measured in whole cell extracts using the luciferase assay system (Promega, E1500). β-galactosidase activity was measured as previously described (Eustice et al., 1991).

QUANTIFICATION AND STATISTICAL ANALYSIS

Quantitative analyses were performed on at least three biological replicates unless otherwise indicated, and the number of replicates (n) are described in the relevant figure legends. GraphPad Prism software (RRID:SCR_002798) version 6.0 was used to analyze the data. Data were analyzed for normal distribution and passed Kolmogorov-Smirnov normality test. Statistical analyses were performed using two-tailed Student's unpaired *t* test for two-group comparisons, or one-way ANOVA for multi-group comparisons. Data are presented as the mean ± standard error of the mean (SEM) unless otherwise indicated in the relevant figure legends. *p* values lower than 0.05 are considered statistically significant.

Supplementary Material

Refer to Web version on PubMed Central for supplementary material.

ACKNOWLEDGMENTS

We thank the Genomics High Throughput Facility and the Institute for Immunology FACS Core Facility at the University of California, Irvine for expert service and Raul Ramos and Maksim Plikus for advice on bead injection. This work was supported by NIH grants R01-GM123731 and R01-AR068074 (X.D.). G.G. was supported by a diversity supplement to R01-GM123731.

REFERENCES

Alexander CM, Goel S, Fakhraldeen SA, and Kim S (2012). Wnt signaling in mammary glands: plastic cell fates and combinatorial signaling. Cold Spring Harb. Perspect. Biol. 4, a008037.

Van Amerongen R, Bowman AN, and Nusse R (2012). Developmental stage and time dictate the fate of Wnt/β-catenin- responsive stem cells in the mammary gland. Cell Stem Cell 11, 387–400. [PubMed: 22863533]

Andl T, Ahn K, Kairo A, Chu EY, Wine-Lee L, Reddy ST, Croft NJ, Cebra-Thomas JA, Metzger D, Chambon P, et al. (2004). Epithelial Bmpr1a regulates differentiation and proliferation in postnatal hair follicles and is essential for tooth development. Development 131, 2257–2268. [PubMed: 15102710]

Arendt LM, and Kuperwasser C (2015). Form and function: how estrogen and progesterone regulate the mammary epithelial hierarchy. J. Mammary Gland Biol. Neoplasia. 20, 9–25. [PubMed: 26188694]

Ballard MS, Zhu A, Iwai N, Stensrud M, Mapps A, Postiglione MP, Knoblich JA, and Hinck L (2015). Mammary stem cell self-renewal is regulated by slit2/robo1 signaling through SNAI1 and mINSC. Cell Rep. 13, 290–301. [PubMed: 26440891]

Behrens J, Jerchow BA, Würtele M, Grimm J, Asbrand C, Wirtz R, Kühl M, Wedlich D, and Birchmeier W (1998). Functional interaction of an axin homolog, conductin, with β-catenin, APC, and GSK3β. Science 280, 596–599. [PubMed: 9554852]

Bolger AM, Lohse M, and Usadel B (2014). Trimmomatic: a flexible trimmer for Illumina sequence data. Bioinformatics 30, 2114–2120. [PubMed: 24695404]

Bouras T, Pal B, Vaillant F, Harburg G, Asselin-Labat ML, Oakes SR, Lindeman GJ, and Visvader JE (2008). Notch signaling regulates mammary stem cell function and luminal cell-fate commitment. Cell Stem Cell 3, 429–441. [PubMed: 18940734]

Brabletz S, and Brabletz T (2010). The ZEB/miR-200 feedback loop-a motor of cellular plasticity in development and cancer? EMBO Rep 11, 670–677. [PubMed: 20706219]

Brabletz S, Lasierra Losada M, Schmalhofer O, Mitschke J, Krebs A, Brabletz T, and Stemmler MP (2017). Generation and characterization of mice for conditional inactivation of Zeb1. Genesis 55. 10.1002/dvg.23024.

Brisken C, Heineman A, Chavarria T, Elenbaas B, Tan J, Dey SK, McMahon JA, McMahon AP, and Weinberg RA (2000). Essential function of Wnt-4 in mammary gland development downstream of progesterone signaling. Genes Dev 14, 650–654. [PubMed: 10733525]

Cai S, Kalisky T, Sahoo D, Dalerba P, Feng W, Lin Y, Qian D, Kong A, Yu J, Wang F, et al. (2017). A quiescent Bcl11b high stem cell population is required for maintenance of the mammary gland. Cell Stem Cell 20, 247–260.e5. [PubMed: 28041896]

Chaffer CL, Marjanovic ND, Lee T, Bell G, Kleer CG, Reinhardt F, D'Alessio AC, Young RA, and Weinberg RA (2013). XPoised chromatin at the ZEB1 promoter enables breast cancer cell plasticity and enhances tumorigenicity. Cell 154, 61–74. [PubMed: 23827675]

Chen Q, Zhang N, Gray RS, Li H, Ewald AJ, Zahnow CA, and Pan D (2014). A temporal requirement for Hippo signaling in mammary gland differentiation, growth, and tumorigenesis. Genes Dev 28, 432–437. [PubMed: 24589775]

Chung CY, Ma Z, Dravis C, Preissl S, Poirion O, Luna G, Hou X, Giraddi RR, Ren B, and Wahl GM (2019). Single-cell chromatin analysis of mammary gland development reveals cell-state transcriptional regulators and lineage relationships. Cell Rep. 29, 495–510.e6. [PubMed: 31597106]

Ciarloni L, Mallepell S, and Brisken C (2007). Amphiregulin is an essential mediator of estrogen receptor α function in mammary gland development. Proc. Natl. Acad. Sci. U S A 104, 5455–5460. [PubMed: 17369357]

Dobin A, Davis CA, Schlesinger F, Drenkow J, Zaleski C, Jha S, Batut P, Chaisson M, and Gingeras TR (2013). STAR: ultrafast universal RNA-seq aligner. Bioinformatics 29, 15–21. [PubMed: 23104886]

Dontu G, Abdallah WM, Foley JM, Jackson KW, Clarke MF, Kawamura MJ, and Wicha MS (2003). In vitro propagation and transcriptional profiling of human mammary stem/progenitor cells. Genes Dev 17, 1253–1270. [PubMed: 12756227]

Eddaoudi A, Canning SL, and Kato I (2018). Flow cytometric detection of g0 in live cells by Hoechst 33342 and Pyronin Y staining. In Methods in Molecular Biology.

Eustice DC, Feldman PA, Colberg-Poley AM, Buckery RM, and Neubauer RH (1991). A sensitive method for the detection of β-galactosidase in transfected mammalian cells. Biotechniques 11, 739–740, 742–3. [PubMed: 1809326]

Feldker N, Ferrazzi F, Schuhwerk H, Widholz SA, Guenther K, Frisch I, Jakob K, Kleemann J, Riegel D, Bö nisch U, et al. (2020). Genome-wide cooperation of EMT transcription factor ZEB 1 with YAP and AP −1 in breast cancer. EMBO J 39, e103209.

Fu NY, Rios AC, Pal B, Law CW, Jamieson P, Liu R, Vaillant F, Jackling F, Liu KH, Smyth GK, et al. (2017). Identification of quiescent and spatially restricted mammary stem cells that are hormone responsive. Nat. Cell Biol. 19, 164–176. [PubMed: 28192422]

Fu NY, Pal B, Chen Y, Jackling FC, Milevskiy M, Vaillant F, Capaldo BD, Guo F, Liu KH, Rios AC, et al. (2018). Foxp1 is indispensable for ductal morphogenesis and controls the exit of mammary stem cells from quiescence. Dev. Cell 47, 629–644.e8. [PubMed: 30523786]

Fu NY, Nolan E, Lindeman GJ, and Visvader JE (2020). Stem cells and the differentiation hierarchy in mammary gland development. Physiol. Rev. 100, 489–523. [PubMed: 31539305]

Fu R, Han CF, Ni T, Di L, Liu LJ, Lv WC, Bi YR, Jiang N, He Y, Li HM, et al. (2019). A ZEB1/p53 signaling axis in stromal fibroblasts promotes mammary epithelial tumours. Nat. Commun. 19, 10–3210.

Glinka A, Wu W, Delius H, Monaghan AP, Blumenstock C, and Niehrs C (1998). Dickkopf-1 is a member of a new family of secreted proteins and functions in head induction. Nature 391, 357–362. [PubMed: 9450748]

Gu B, Sun P, Yuan Y, Moraes RC, Li A, Teng A, Agrawal A, Rhéaume C, Bilanchone V, Veltmaat JM, et al. (2009). Pygo2 expands mammary progenitor cells by facilitating histone H3 K4 methylation. J. Cell Biol. 185, 811–826. [PubMed: 19487454]

Gu B, Watanabe K, Sun P, Fallahi M, and Dai X (2013). Chromatin effector Pygo2 mediates wnt-notch crosstalk to suppress luminal/alveolar potential of mammary stem and basal cells. Cell Stem Cell 13, 48–61. [PubMed: 23684539]

Guo W, Keckesova Z, Donaher JL, Shibue T, Tischler V, Reinhardt F, Itzkovitz S, Noske A, Zürrer-Härdi U, Bell G, et al. (2012). Slug and Sox9 cooperatively determine the mammary stem cell state. Cell 148, 1015–1028. [PubMed: 22385965]

Haensel D, and Dai X (2018). Epithelial-to-mesenchymal transition in cutaneous wound healing: where we are and where we are heading. Dev. Dyn.247, 473–480. [PubMed: 28795450]

Haensel D, Jin S, Sun P, Cinco R, Dragan M, Nguyen Q, Cang Z, Gong Y, Vu R, MacLean AL, et al. (2020). Defining epidermal basal cell states during skin homeostasis and wound healing using single-cell transcriptomics. Cell Rep 30, 3932–3947.e6. [PubMed: 32187560]

He TC, Sparks AB, Rago C, Hermeking H, Zawel L, Da Costa LT, Morin PJ, Vogelstein B, and Kinzler KW (1998). Identification of c-MYC as a target of the APC pathway. Science 281, 1509–1512. [PubMed: 9727977]

Hong T, Watanabe K, Ta CH, Villarreal-Ponce A, Nie Q, and Dai X (2015). An ovol2-Zeb1 mutual inhibitory circuit governs bidirectional and multi-step transition between epithelial and mesenchymal states. PLoS Comput. Biol. 11, e1004569.

Hovanes K, Li TWH, Munguia JE, Truong T, Milovanovic T, Lawrence Marsh J, Holcombe RF, and Waterman ML (2001). β-Catenin-sensitive isoforms of lymphoid enhancer factor-1 are selectively expressed in colon cancer. Nat. Genet. 28, 53–57. [PubMed: 11326276]

Inman JL, Robertson C, Mott JD, and Bissell MJ (2015). Mammary gland development: cell fate specification, stem cells and the microenvironment. Dev 142, 1028–1042.

Jardé T, Lloyd-Lewis B, Thomas M, Kendrick H, Melchor L, Bougaret L, Watson PD, Ewan K, Smalley MJ, and Dale TC (2016). Wnt and neuregulin1/ErbB signalling extends 3D culture of hormone responsive mammary organoids. Nat. Commun. 7, 13207. [PubMed: 27782124]

Jho E, Zhang T, Domon C, Joo C-K, Freund J-N, and Costantini F (2002). Wnt/β-Catenin/Tcf signaling induces the transcription of Axin2, a negative regulator of the signaling pathway. Mol. Cell. Biol. 22, 1172–1183. [PubMed: 11809808]

Kalailingam P, Tan HB, Jain N, Sng MK, Chan JSK, Tan NS, and Thanabalu T (2017). Conditional knock out of N-WASP in keratinocytes causes skin barrier defects and atopic dermatitis-like inflammation. Sci. Rep. 7, 7311. [PubMed: 28779153]

Keller PJ, Lin AF, Arendt LM, Klebba I, Jones AD, Rudnick JA, Di-Meo TA, Gilmore H, Jefferson DM, Graham RA, et al. (2010). Mapping the cellular and molecular heterogeneity of normal and malignant breast tissues and cultured cell lines. Breast Cancer Res 12, R87. [PubMed: 20964822]

Van Keymeulen A, Rocha AS, Ousset M, Beck B, Bouvencourt G, Rock J, Sharma N, Dekoninck S, and Blanpain C (2011). Distinct stem cells contribute to mammary gland development and maintenance. Nature 479, 189–193. [PubMed: 21983963]

Kim KH, and Sederstrom JM (2015). Assaying cell cycle status using flow cytometry. Curr. Protoc. Mol. Biol. 111, 28.6.1–28.6.11.

Lee B, Villarreal-Ponce A, Fallahi M, Ovadia J, Sun P, Yu Q-C, Ito S, Sinha S, Nie Q, and Dai X (2014). Transcriptional mechanisms link epithelial plasticity to adhesion and differentiation of epidermal progenitor cells. Dev. Cell 29, 47–58. [PubMed: 24735878]

Lehmann W, Mossmann D, Kleemann J, Mock K, Meisinger C, Brummer T, Herr R, Brabletz S, Stemmler MP, and Brabletz T (2016). ZEB1 turns into a transcriptional activator by interacting with YAP1 in aggressive cancer types. Nat. Commun. 7, 10498.

Lim E, Wu D, Pal B, Bouras T, Asselin-Labat ML, Vaillant F, Yagita H, Lindeman GJ, Smyth GK, and Visvader JE (2010). Transcriptome analyses of mouse and human mammary cell subpopulations reveal multiple conserved genes and pathways. Breast Cancer Res 12, R21. [PubMed: 20346151]

Lindley LE, Curtis KM, Sanchez-Mejias A, Rieger ME, Robbins DJ, and Briegel KJ (2015). The WNT-controlled transcriptional regulator LBH is required for mammary stem cell expansion and maintenance of the basal lineage. Dev. 142, 893–904.

Liu S, Dontu G, and Wicha MS (2005). Mammary stem cells, self-renewal pathways, and carcinogenesis. Breast Cancer Res 7, 86–95. [PubMed: 15987436]

Liu W, Wu T, Dong X, and Zeng YA (2017). Neuropilin-1 is upregulated by Wnt/β-catenin signaling and is important for mammary stem cells. Sci. Rep. 7, 10941. [PubMed: 28887477]

Lloyd-Lewis B, Davis FM, Harris OB, Hitchcock JR, and Watson CJ (2018). Neutral lineage tracing of proliferative embryonic and adultmammary stem/progenitor cells. Dev 145, dev164079.

Love MI, Huber W, and Anders S (2014). Moderated estimation of fold change and dispersion for RNA-seq data with DESeq2. Genome Biol 15, 550. [PubMed: 25516281]

Lowry WE, Blanpain C, Nowak JA, Guasch G, Lewis L, and Fuchs E (2005). Defining the impact of β-catenin/Tcf transactivation on epithelial stem cells. Genes Dev 19, 1596–1611. [PubMed: 15961525]

Macias H, Moran A, Samara Y, Moreno M, Compton JE, Harburg G, Strickland P, and Hinck L (2011). SLIT/ROBO1 signaling suppresses mammary branching morphogenesis by limiting basal cell number. Dev. Cell. 20, 827–840. [PubMed: 21664580]

Mani SA, Guo W, Liao MJ, Eaton EN, Ayyanan A, Zhou AY, Brooks M, Reinhard F, Zhang CC, Shipitsin M, et al. (2008). The epithelial-mesen-chymal transition generates cells with properties of stem cells. Cell 133, 704–715. [PubMed: 18485877]

Meijer L, Skaltsounis AL, Magiatis P, Polychronopoulos P, Knockaert M, Leost M, Ryan XP, Vonica CA, Brivanlou A, Dajani R, et al. (2003). GSK-3-Selective inhibitors derived from Tyrian purple indirubins. Chem. Biol 10, 1255–1266. [PubMed: 14700633]

Morel AP, Liè vre M, Thomas C, Hinkal G, Ansieau S, and Puisieux A (2008). Generation of breast cancer stem cells through epithelial-mesen-chymal transition. PLoS One.

Nassour M, Idoux-Gillet Y, Selmi A, Côme C, Faraldo MLM, Deugnier MA, and Savagner P (2012). Slug controls stem/progenitor cell growth dynamics during mammary gland morphogenesis. PLoS One 7, e53498.

Neve RM, Chin K, Fridlyand J, Yeh J, Baehner FL, Fevr T, Clark L, Bayani N, Coppe JP, Tong F, et al. (2006). A collection of breast cancer cell lines for the study of functionally distinct cancer subtypes. Cancer Cell 10, 515–527. [PubMed: 17157791]

Nguyen QH, Pervolarakis N, Blake K, Ma D, Davis RT, James N, Phung AT, Willey E, Kumar R, Jabart E, et al. (2018). Profiling human breast epithelial cells using single cell RNA sequencing identifies cell diversity. Nat. Commun. 9, 2028. [PubMed: 29795293]

Nieto MA, Huang RYYJ, Jackson RAA, and Thiery JPP (2016). EMT: 2016. Cell 30, 21–45. 10.1016/j.cell.2016.06.028.

Pal B, Chen Y, Vaillant F, Jamieson P, Gordon L, Rios AC, Wilcox S, Fu N, Liu KH, Jackling FC, et al. (2017). Construction of developmental lineage relationships in the mouse mammary gland by single-cell RNA profiling. Nat. Commun. 8, 1627. [PubMed: 29158510]

Pastushenko I, and Blanpain C (2019). EMT transition states during tumor progression and metastasis. Trends Cell Biol. 29, 212–226. [PubMed: 30594349]

Pervolarakis N, Nguyen QH, Williams J, Gong Y, Gutierrez G, Sun P, Jhutty D, Zheng GXY, Nemec CM, Dai X, et al. (2020). Integrated single-cell transcriptomics and chromatin accessibility analysis reveals regulators of mammary epithelial cell identity. Cell Rep. 33, 108273.

Plaks V, Brenot A, Lawson DA, Linnemann JR, Van Kappel EC, Wong KC, de Sauvage F, Klein OD, and Werb Z (2013). Lgr5-Expressing cells are sufficient and necessary for postnatal mammary gland organogenesis. Cell Rep. 3, 70–78. [PubMed: 23352663]

Prater MD, Petit V, Alasdair Russell I, Giraddi RR, Shehata M, Menon S, Schulte R, Kalajzic I, Rath N, Olson MF, et al. (2014). Mammary stem cells have myoepithelial cell properties. Nat. Cell Biol. 16, 942–950, 1–7. [PubMed: 25173976]

Qu Y, Han B, Yu Y, Yao W, Bose S, Karlan BY, Giuliano AE, and Cui X (2015). Evaluation of MCF10A as a reliable model for normal human mammary epithelial cells. PLoS One 10, e0131285.

Richter J, Traver D, and Willert K (2017). The role of Wnt signaling in hematopoietic stem cell development. Crit. Rev. Biochem. Mol. Biol. 52, 414–424. [PubMed: 28508727]

Rios AC, Fu NY, Lindeman GJ, and Visvader JE (2014). In situ identification of bipotent stem cells in the mammary gland. Nature 506, 322–327. [PubMed: 24463516]

Roarty K, Shore AN, Creighton CJ, and Rosen JM (2015). Ror2 regulates branching, differentiation, and actincytoskeletal dynamics within the mammary epithelium. J. Cell Biol. 208, 351–366. [PubMed: 25624393]

Röhrs S, Kutzner N, Vlad A, Grunwald T, Ziegler S, and Müller O (2009). Chronological expression of wnt target genes Ccnd1, Myc, Cdkn1a, Tfrc, Plf1 and Ramp3. Cell Biol. Int. 33, 501–508. [PubMed: 19353769]

Sarrió D, Rodriguez-Pinilla SM, Hardisson D, Cano A, Moreno-Bueno G, and Palacios J (2008). Epithelial-mesenchymal transition in breast cancer relates to the basal-like phenotype. Cancer Res 68, 989–997. [PubMed: 18281472]

Sha Y, Haensel D, Gutierrez G, Du H, Dai X, and Nie Q (2019). Intermediate cell states in epithelial-to-mesenchymal transition. Phys. Biol. 16.

Shackleton M, Vaillant F, Simpson KJ, Stingl J, Smyth GK, Asselin-Labat ML, Wu L, Lindeman GJ, and Visvader JE (2006). Generation of a functional mammary gland from a single stem cell. Nature 439, 84–88. [PubMed: 16397499]

Sikandar SS, Kuo AH, Kalisky T, Cai S, Zabala M, Hsieh RW, Lobo NA, Scheeren FA, Sim S, Qian D, et al. (2017). Role of epithelial to mesen-chymal transition associated genes in mammary gland regeneration and breast tumorigenesis. Nat. Commun. 8, 1669. [PubMed: 29162812]

Stemmler MP, Eccles RL, Brabletz S, and Brabletz T (2019). Non-redundant functions of EMT transcription factors. Nat. Cell Biol. 21, 102–112. [PubMed: 30602760]

Sternlicht MD, Kouros-Mehr H, Lu P, and Werb Z (2006). Hormonal and local control of mammary branching morphogenesis. Differentiation 74, 365–381. [PubMed: 16916375]

Stingl J, Eirew P, Ricketson I, Shackleton M, Vaillant F, Choi D, Li HI, and Eaves CJ (2006). Purification and unique properties of mammary epithelial stem cells. Nature 439, 993–997. [PubMed: 16395311]

Sun H, Miao Z, Zhang X, Chan UI, Su SM, Guo S, Wong CKH, Xu X, and Deng CX (2018). Single-cell RNA-Seq reveals cell heterogeneity and hierarchy within mouse mammary epithelia. J. Biol. Chem. 293, 8315–8329. [PubMed: 29666189]

Thiery JP, Acloque H, Huang RYJ, and Nieto MA (2009). Epithelial-mesenchymal transitions in development and disease. Cell.

Unezaki S, Horai R, Sudo K, Iwakura Y, and Ito S (2007). Ovol2/Movo, a homologue of Drosophila ovo, is required for angiogenesis, heart formation and placental development in mice. Genes Cells 12, 773–785. [PubMed: 17573777]

Wang D, Cai C, Dong X, Yu QC, Zhang XO, Yang L, and Zeng YA (2015). Identification of multipotent mammary stemcells by protein C receptor expression. Nature 517, 81–84. [PubMed: 25327250]

Wang X, Xu H, Cheng C, Ji Z, Zhao H, Sheng Y, Li X, Wang J, Shu Y, He Y, et al. (2020). Identification of a Zeb1 expressing basal stem cell subpopulation in the prostate. Nat. Commun. 11, 706. [PubMed: 32024836]

Watanabe K, Villarreal-Ponce A, Sun P, Salmans ML, Fallahi M, Andersen B, and Dai X (2014). Mammary morphogenesis and regeneration require the inhibition of EMT at terminal end buds by ovol2 transcriptional repressor. Dev. Cell 29, 59–74. [PubMed: 24735879]

Watson CJ (2021). How should we define mammary stem cells? Trends Cell Biol. 31, 621–627. [PubMed: 33902986]

Watson CJ, and Khaled WT (2008). Mammary development in the embryo and adult: a journey of morphogenesis and commitment. Development 135, 995–1003. [PubMed: 18296651]

Watson CJ, and Khaled WT (2020). Mammary development in the embryo and adult: new insights into the journey of morphogenesis and commitment. Development 147, dev169862.

Wells J, Lee B, Cai AQ, Karapetyan A, Lee W-J, Rugg E, Sinha S, Nie Q, and Dai X (2009). Ovol2 suppresses cell cycling and terminal differentiation of keratinocytes by directly repressing c-Myc and Notch1. J. Biol. Chem. 284, 29125–29135. [PubMed: 19700410]

Welm BE, Dijkgraaf GJP, Bledau AS, Welm AL, and Werb Z (2008). Lentiviral Transduction of mammary stem cells for analysis of gene function during development and cancer. Cell Stem Cell 2, 90–102. [PubMed: 18371425]

Woodward WA, Chen MS, Behbod F, and Rosen JM (2005). On mammary stem cells. J. Cell Sci. 118 (Pt 16), 3585–3594. [PubMed: 16105882]

Wuidart A, Ousset M, Rulands S, Simons BD, Van Keymeulen A, and Blanpain C (2016). Quantitative lineage tracing strategies to resolve multipotency in tissue-specific stem cells. Genes Dev 30, 1261–1277. [PubMed: 27284162]

Xu J, Lamouille S, and Derynck R (2009). TGF-B-induced epithelial to mesenchymal transition. Cell Res. 19, 156–172. [PubMed: 19153598]

Yang J, Mani SA, Donaher JL, Ramaswamy S, Itzykson RA, Come C, Savagner P, Gitelman I, Richardson A, and Weinberg RA (2004). Twist, a master regulator of morphogenesis, plays an essential role in tumor metastasis. Cell 117, 927–939. [PubMed: 15210113]

Yang J, Antin P, Berx G, Blanpain C, Brabletz T, Bronner M, Campbell K, Cano A, Casanova J, Christofori G, et al. (2020). Guidelines and definitions for research on epithelial–mesenchymal transition. Nat. Rev. Mol. Cell Biol. 21, 341–352. [PubMed: 32300252]

Ye X, Tam WL, Shibue T, Kaygusuz Y, Reinhardt F, Ng Eaton E, and Weinberg RA (2015). Distinct EMT programs control normal mammary stem cells and tumour-initiating cells. Nature 525, 256–260. [PubMed: 26331542]

Zeng YA, and Nusse R (2010). Wnt proteins are self-renewal factors for mammary stem cells and promote their long-term expansion in culture. Cell Stem Cell 6, 568–577. [PubMed: 20569694]

Highlights

- Maintenance of mammary basal cell fate and stem cell quiescence requires Zeb1
- Zeb1 promotes basal cell fate in part through EMT-associated gene regulation
- Zeb1 acts in quiescent basal cells to promote self-renewal and suppress proliferation
- Zeb1 suppression of Wnt signaling is important for basal stem cell maintenance

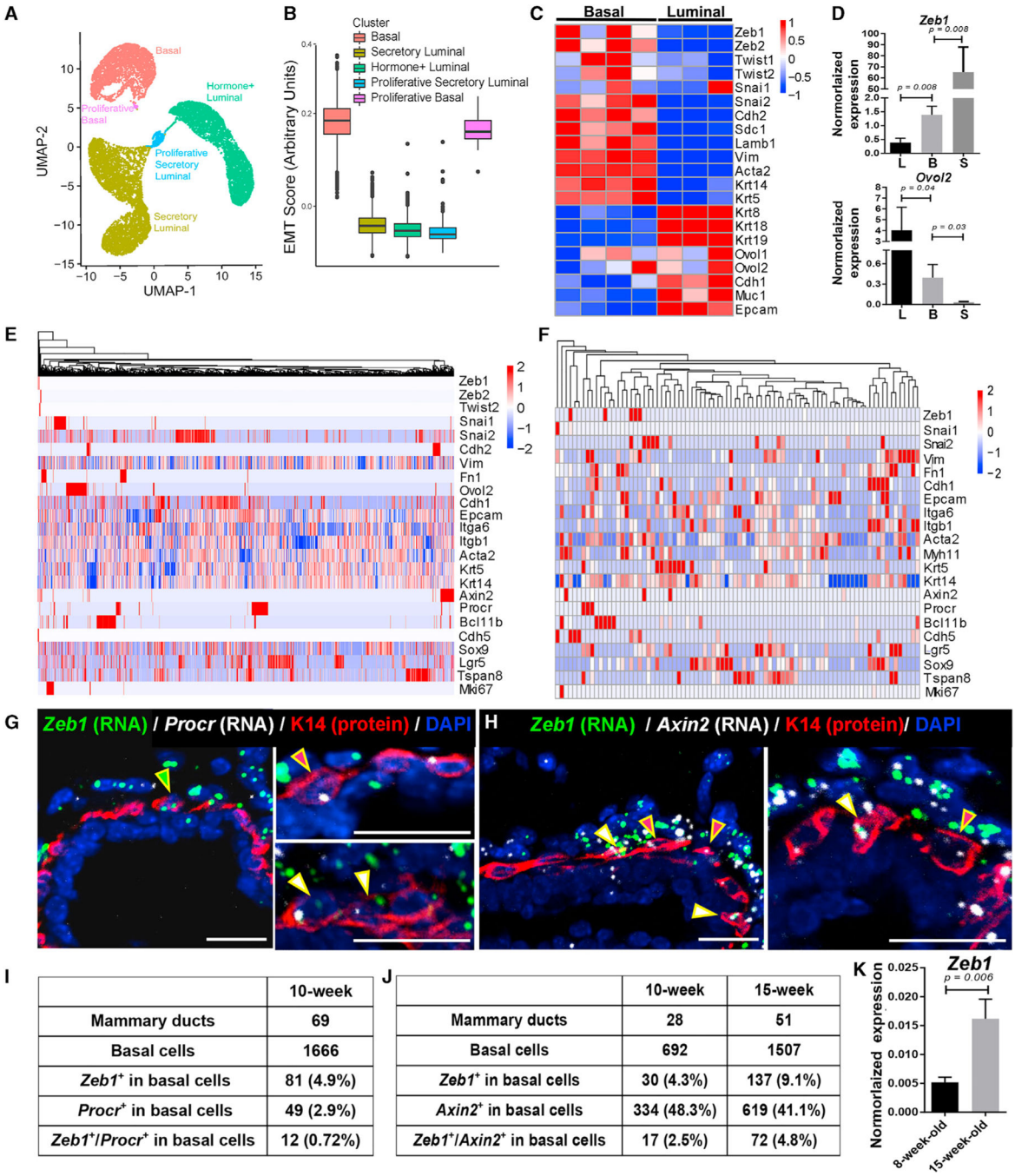

	10-week
Mammary ducts	69
Basal cells	1666
Zeb1$^+$ in basal cells	81 (4.9%)
Procr$^+$ in basal cells	49 (2.9%)
Zeb1$^+$/*Procr*$^+$ in basal cells	12 (0.72%)

	10-week	15-week
Mammary ducts	28	51
Basal cells	692	1507
Zeb1$^+$ in basal cells	30 (4.3%)	137 (9.1%)
Axin2$^+$ in basal cells	334 (48.3%)	619 (41.1%)
Zeb1$^+$/*Axin2*$^+$ in basal cells	17 (2.5%)	72 (4.8%)

Figure 1. Expression of EMT-associated genes and identification of *Zeb1*-expressing basal cells in the mammary epithelium

(A) Uniform Manifold Approximation and Projection (UMAP) of the distinct epithelial cell clusters identified in 8- to 9-week-old MGs.

(B) Boxplots displaying differential expression of an EMT gene signature in the identified cell clusters. See Table S2 for the list of genes used for scoring.

(C) Heatmap of DNA microarray data (Gu et al., 2013) showing differential expression of the indicated genes in Lin$^-$CD24$^+$CD49^{high} basal and Lin$^-$CD24$^+$CD49^{low} luminal cells from 8- to 12-week-old mice.

(D) qRT-PCR analysis of *Zeb1* and *Ovol2* expression in Lin^{-}CD49f^{high}EpCAM^{+} basal, Lin^{-}CD49f^{high}EpCAM ^{high} luminal, and Lin^{-}CD49f^{low}EpCAM^{-} stromal cell populations from 12-week-old mice (n = 3).

(E and F) Heatmaps showing the expression enrichment of individual EMT-associated genes and known SC markers in basal MECs sequenced with the 10× (E) or C1 (F) platform. The color code shows the expression level in each cell relative to the average expression level in all cells (e.g., red indicates a cell that expresses a higher level of a particular gene than the average and white indicates the average).

(G and H) RNAScope images showing co-analysis of *Zeb1* with *Procr* (G) or *Axin2* (H) mRNAs in MGs from 10-week-old mice. K14 antibody highlights the basal MECs. DAPI stains the nuclei. Arrowheads point to the cells positive for one or both signals.

(I and J) Quantitative analysis of the RNAScope data on MGs from 10-week-old or 15-week-old (see Figure S1H) mice.

(K) qRT-PCR analysis of *Zeb1* expression in Lin^{-}CD49f^{high}EpCAM^{+} basal MECs from 8-week-old or 15-week-old mice (n = 3 each).

Scale bars: 50 μm in (G) and (H). See also Figure S1 and Tables S1, S2, S4, and S5.

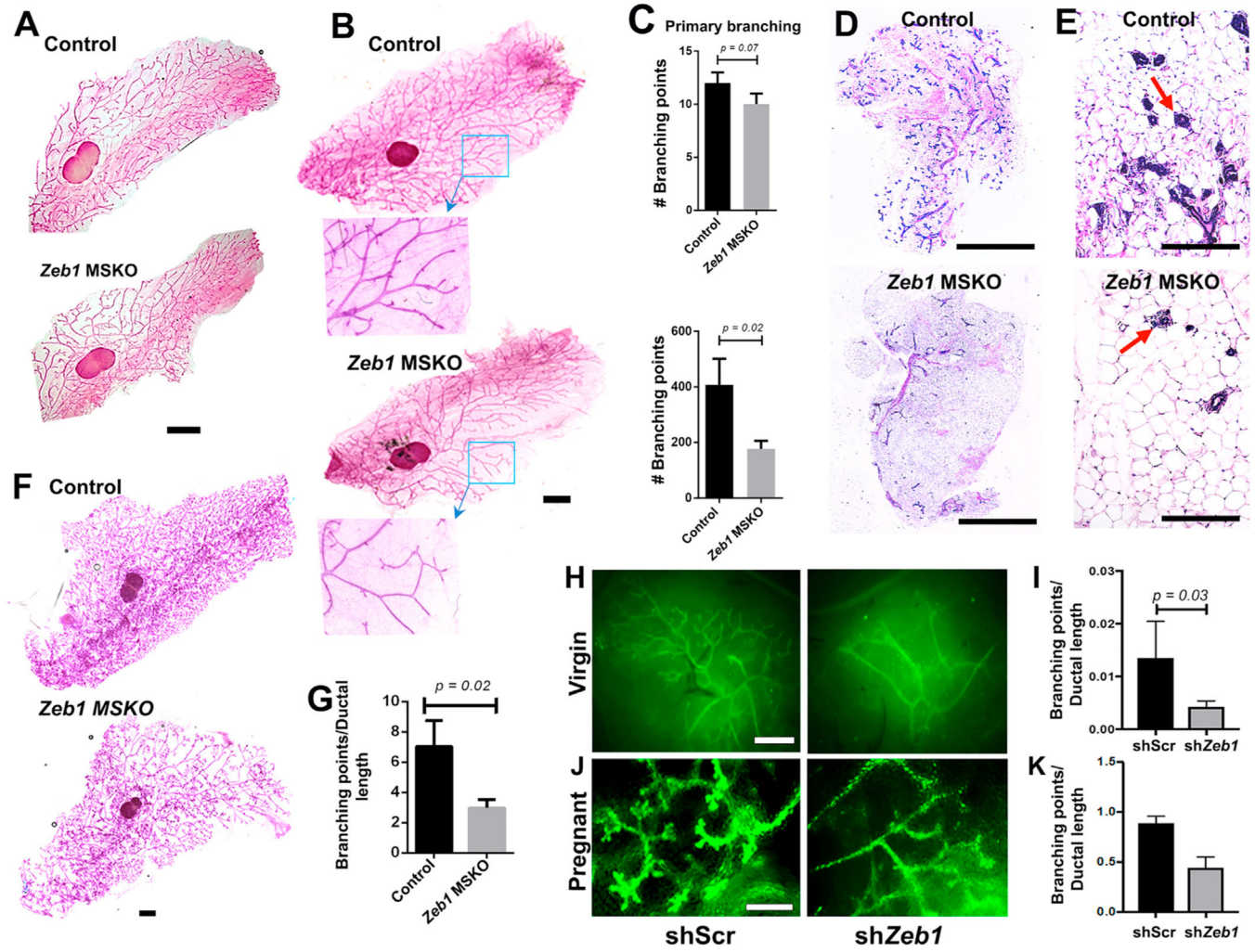

Figure 2. MEC-specific *Zeb1* deficiency compromises ductal branching morphogenesis (A–C) Whole-mount analysis of MGs from 8-week-old

(A) and 17-week-old (B and C) virgin *K14-Cre*;*Zeb1*$^{f/+}$ (control) and *K14-Cre*;*Zeb1*$^{f/f}$ (MSKO) mice. Boxed areas in (B) are shown at higher magnification.

(D and E) H&E images of MGs from 17-week-old virgin control and MSKO mice. Arrows indicate individual ductal sections.

(F and G) Whole-mount analysis of MGs from pregnant (P14.5) control and MSKO mice. Representative images are shown in (A), (B), and (F), and quantification from multiple pairs are shown in (C) (n = 3) and (G) (n = 3).

(H–K) Results of cleared fat pad transplantation of FACS-sorted basal MECs infected with lentiviruses that express shScr or sh*Zeb1*. (H) and (J) show representative images of transplants from virgin hosts analyzed at 8 weeks after transplantation (H) or hosts that were subsequently mated to WT males (J). (I) and (K) show summary of data for (H) (n = 5) and (J) (n = 2), respectively. Data presented here were obtained using sh*Zeb1*-1, and similar results were obtained using sh*Zeb1*-2 (Figures S2J–S2M).

Scale bars: 5 mm in (A), (B), and (F), 1 mm in (D), 100 μm in (E), and 5 mm in (H) and (J).

See also Figure S2.

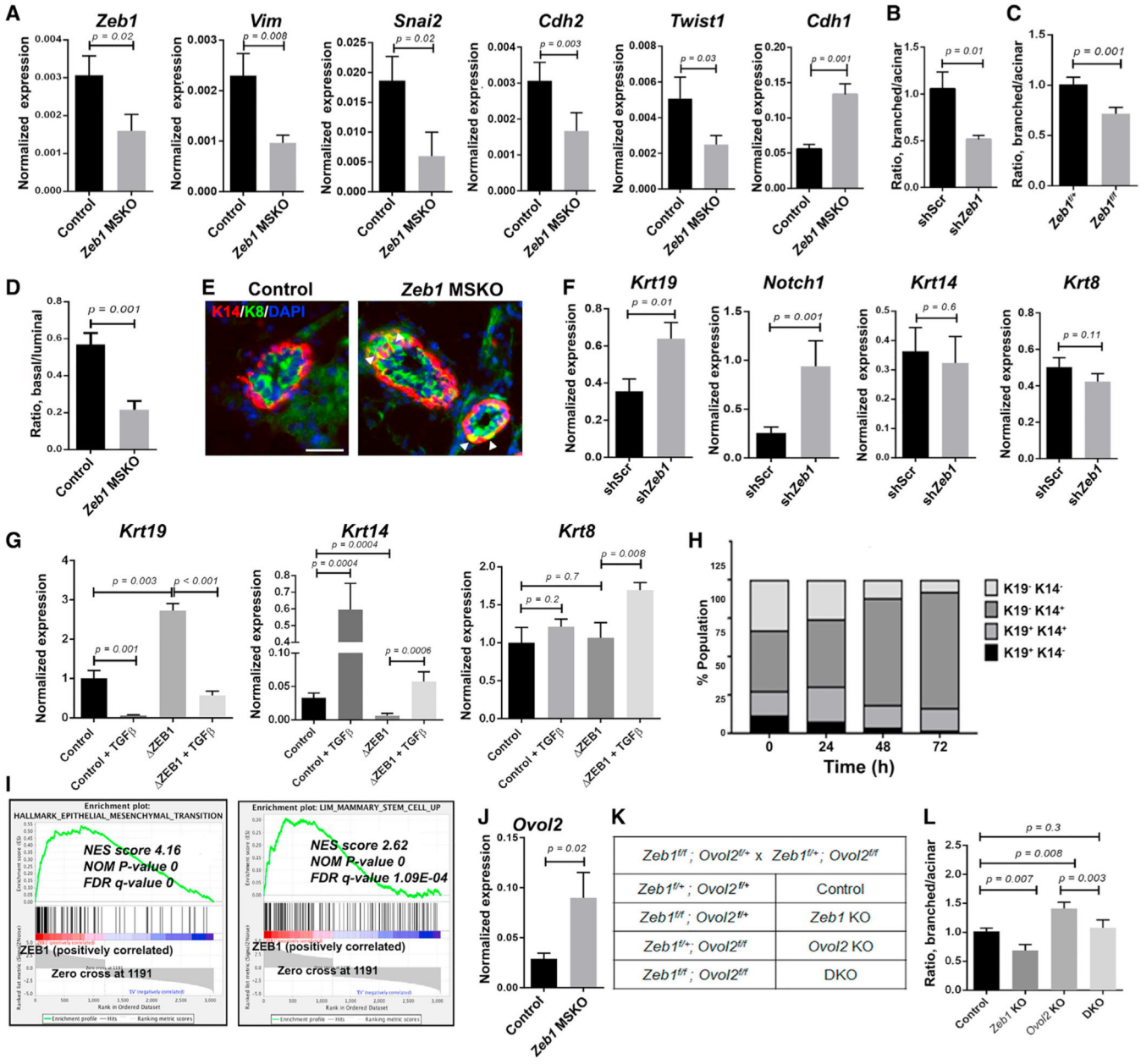

Figure 3. Zeb1/ZEB1 controls basal-luminal balance through EMT-related gene regulation

(A) qRT-PCR analysis of the indicated genes in FACS-sorted basal MECs from 8- to 9-week-old females.

(B) Quantification of organoid types generated by control and *Zeb1*-depleted MECs. Data presented here were obtained using sh*Zeb1*-1, and similar results were obtained using sh*Zeb1*-2 (see Figures S3C and S3D).

(C) Quantification of organoid types generated by Ade-Cre-infected *Zeb1*$^{f/+}$ or *Zeb1*$^{f/f}$ MECs. Data in (B) and (C) are from 3 to 4 independent experiments, respectively.

(D) Flow cytometry quantification of the ratio between basal and luminal MECs in MGs from 12- to 17-week-old *Zeb1* MSKO virgin females and control littermates (n = 5 pairs). See Figure S3H for representative flow plots and absolute cell number.

(E) K14/K8 immunostaining of MGs from 15-week-old *Zeb1* MSKO virgin females and control littermates. Arrowheads indicate K14/K8 double-positive cells in the basal layer. DAPI stains the nuclei. See Figure S3J for summary of data from n = 3 pairs. Scale bar: 50 μm.

(F) qRT-PCR analysis of the indicated genes in control and *Zeb1*-depleted organoids as in (B).

(G) qRT-PCR analysis of the indicated genes in control and *ZEB1*-deleted MCF10A cells. Data are presented as the mean ± standard deviation (SD).

(H) Analysis of keratin protein expression in MCF10A cells at different time points after induction of *Zeb1* overexpression.

(I) Gene set enrichment analysis (GSEA) of RNA-seq data on MCF10A cells (see Table S3 for a complete list of genes used for analysis). FDR, false discovery rate; NES, normalized enrichment score; NOM, nominal.

(J) qRT-PCR analysis of Ovol2 expression in control and *Zeb1* MSKO basal MECs.

(K and L) Organoid formation by control, *Zeb1* single, *Ovol2* single, and *Zeb1*/*Ovol2* double KO (DKO) MECs. Breeding strategy and mouse genotypes are shown in (K), and results of quantification are shown in (L) (n = 3 for each).

See also Figure S3 and Table S3.

A

	Number of cells injected	Number of outgrowths	Fat pad filled
Scramble	20000	7/8	X6 X1 X1
	10000	6/6	X3 X1 X2
	5000	7/8	X2 X2 X3 X1
Zeb1 KD	20000	0/8	X8
	10000	0/8	X8
	5000	0/4	X4

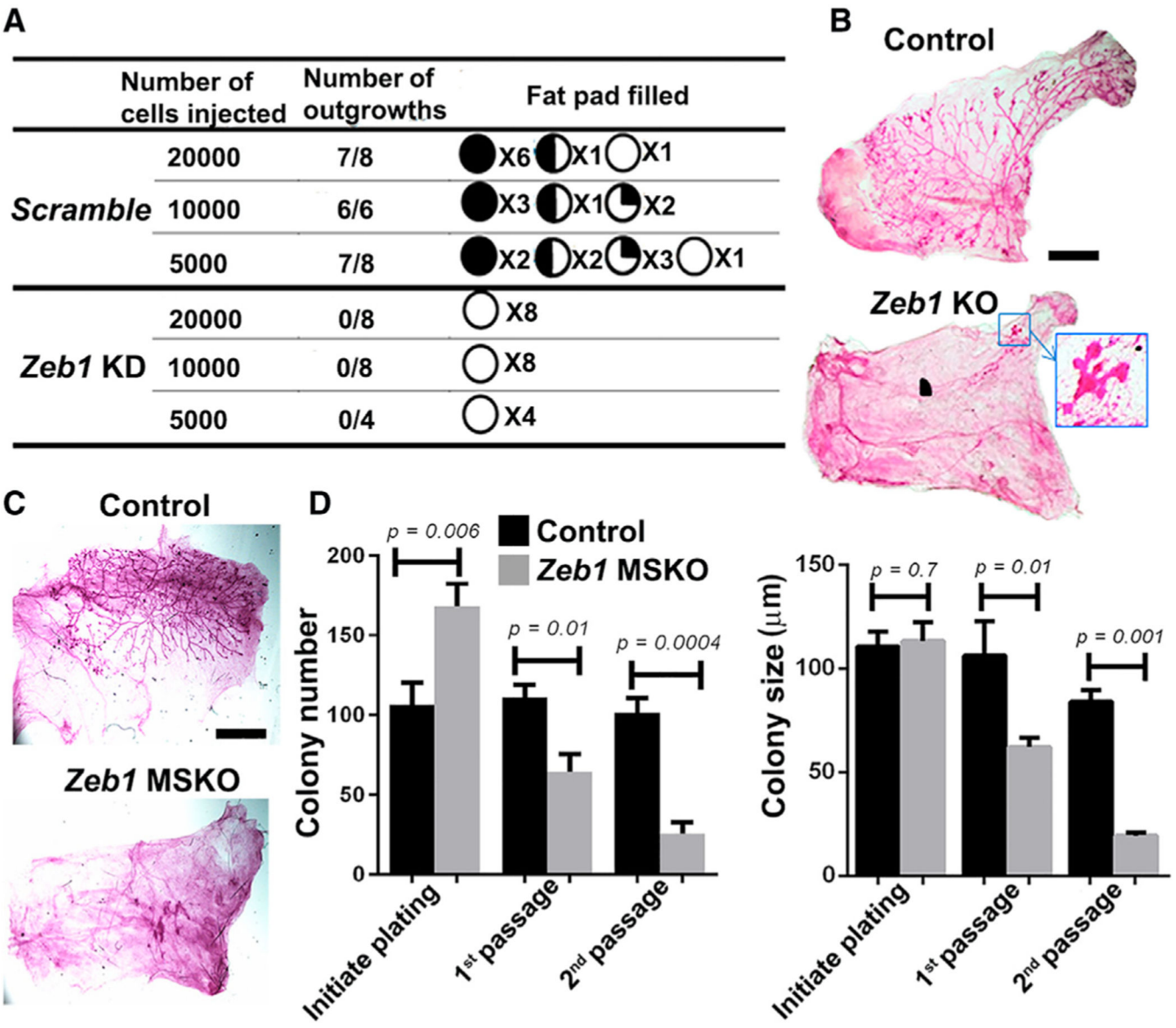

Figure 4. Basal MECs require *Zeb1* for regeneration *in vivo* and clonogenicity *ex vivo*

(A) Limiting dilution transplantation of control and *Zeb1*-depleted basal MECs. The pie charts show approximate take rate and percent fat pad filled by the mammary outgrowths.

(B) Transplants derived from Ade-Cre-infected (GFP^+) basal MECs from 8-week-old $Zeb1^{f/+}$ (control) and $Zeb1^{f/f}$ (KO) mice. See Figure S4B for additional replicates. Boxed area in (B) is shown at higher magnification.

(C) Transplants derived from basal MECs from 8-week-old control and *Zeb1* MSKO mice. Data are representative of n = 3 pairs.

(D) Colony formation by basal MECs from 8-week-old control and *Zeb1* MSKO mice. Shown is a summary from 3 independent experiments. Scale bars: 5 mm in (B) and (C). See Figure S4D for representative colony images.

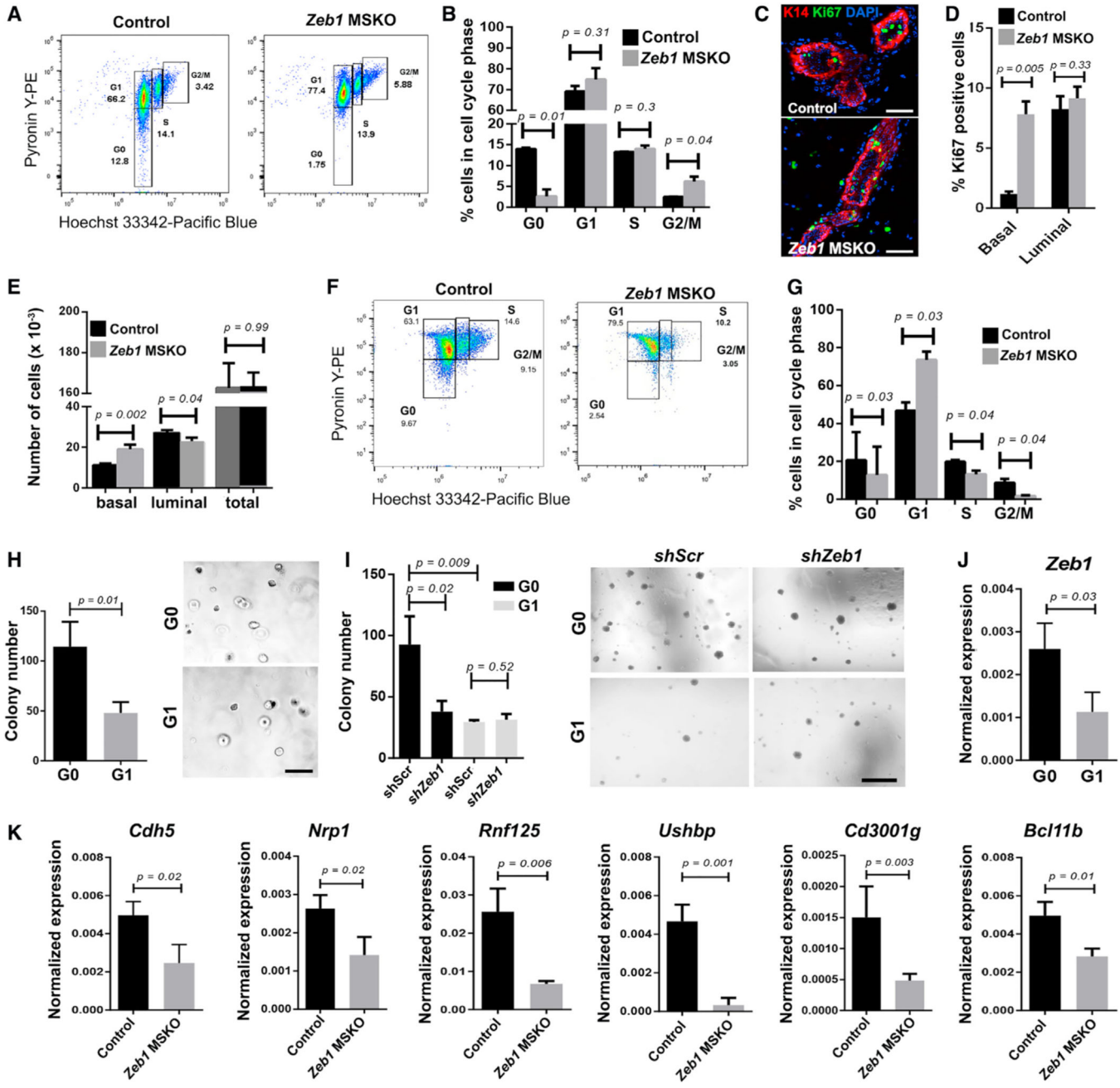

Figure 5. *Zeb1*-deficient basal MECs exhibit defects in cell cycle, quiescence, and G0-associated gene expression

(A and B) Cell cycle analysis of basal MECs from 8- to 9-week-old control and *Zeb1* MSKO mice. Shown are represented FACS profiles of one pair (A) and summary of data from 4 pairs (B) of mice.

(C and D) Ki67 immunostaining in MGs of 8-week-old control and *Zeb1* MSKO mice. Representative images are shown in (C), and summary of data from 3 pairs of mice is shown in (D). K14 antibody stains the basal layer, and DAPI stains the nuclei.

(E) Quantification of the numbers of basal and luminal cells in MGs from 8- to 9-week-old control and *Zeb1* MSKO mice (n = 6 each).

(F and G) Cell cycle analysis of basal MECs in 12-week-old control and *Zeb1* MSKO mice. n = 3 in (G). Boxes in (A) and (F) indicate gating information.
(H and I) Colony formation by G0 and G1 basal MECs with (I, sh*Zeb1*) or without (H, untreated; I, shScr) *Zeb1* depletion. n = 3 each.
(J) qRT-PCR analysis of *Zeb1* expression in sorted G0 and G1 cells. n = 3 each.
(K) qRT-PCR analysis of the indicated genes in basal MECs from 8-week-old control and *Zeb1* MSKO mice. n = 3 pairs.
Scale bars: 50 μm in (C), 500 mm in (H), and 500 μm in (I). See also Figure S5 and Table S7.

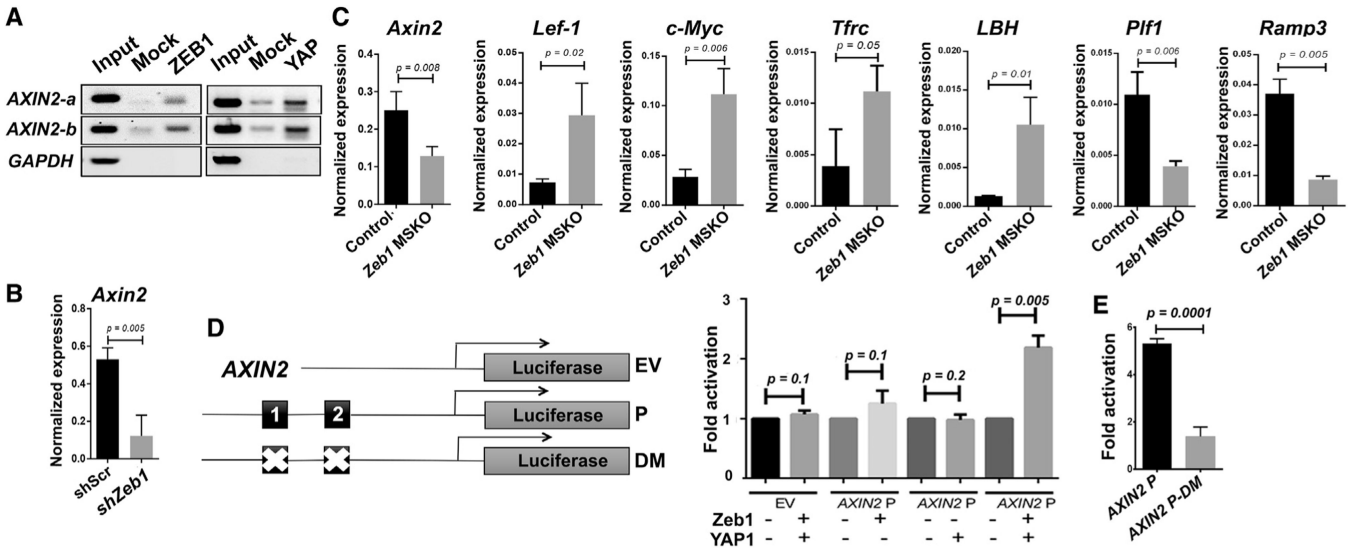

Figure 6. Identification of *Axin2* as a direct target of *Zeb1*/YAP transcriptional activation

(A) ChIP-PCR analysis showing ZEB1 and YAP binding to the same enhancer site upstream of *AXIN2* promoter in MDA-MB-231 cells. *GAPDH* served as a negative control. Shown are data representative of 3 independent experiments.

(B and C) qRT-PCR analysis of the indicated genes in control and *Zeb1*-depleted (B; n = 4) or *Zeb1*-deleted (C; n = 3) basal MECs derived from 12-week-old mice.

(D and E) ZEB1 and YAP1 cooperate to activate the WT (D), but not ZEB1-binding-deficient (E), *AXIN2* enhancer. Diagrams of promoter constructs are shown in (D). Black boxes denote E-box motifs. DM, deletion mutant; EV, empty vector; P, promoter.

See also Figure S6.

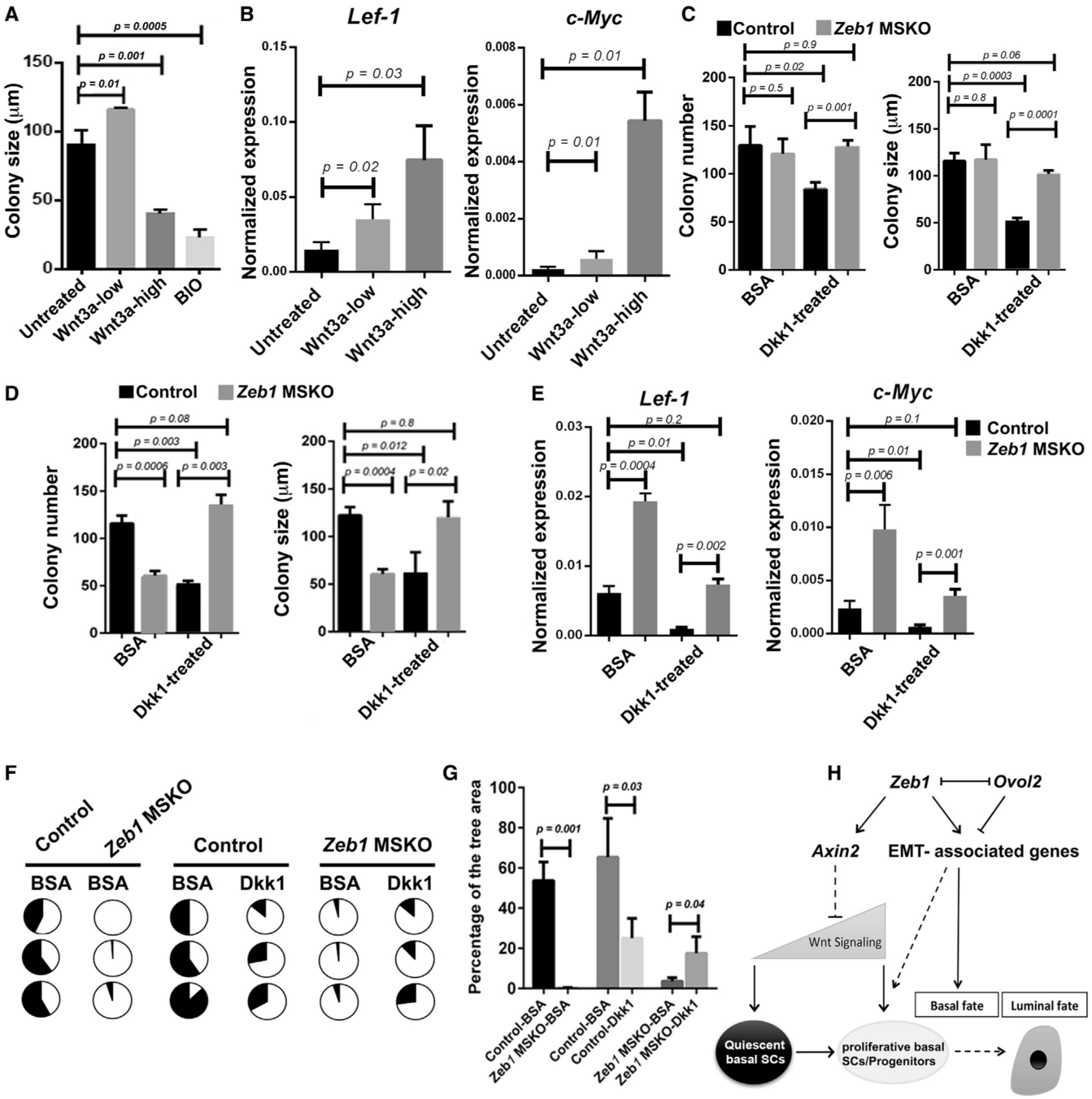

Figure 7. Inhibition of Wnt signaling rescues *Zeb1*-deficiency-induced basal MEC defects *ex vivo* and *in vivo*

(A) Colony formation by WT basal MECs with and without Wnt3a (low, 20 ng/mL; high, 200 ng/mL) or BIO (400 ng/mL). Results were from 3 independent experiments.

(B) qRT-PCR analysis of colonies as in (A).

(C and D) Colony formation by basal MECs from 8-week-old (C) and 15-week-old (D) control and *Zeb1* MSKO mice in the absence or presence of Dkk1 (300 ng/mL). BSA served as a control. n = 3 for each genotype/condition.

(E) qRT-PCR analysis of colonies as in (D).

(F and G) Fat pad transplantation of Dkk1-bead- or BSA-bead-pretreated basal MECs from 15-week-old control and *Zeb1* MSKO mice. Shown are results summarized from 3 independent experiments, with the pie charts displaying percent fat pad filled in each transplant (F) and the graph showing average percentage for all transplants in each condition (G).

(H) Working model on *Zeb1*'s role in mammary basal cell fate and SC control. Solid and dashed lines indicate known/proven and inferred regulations, respectively.

See also Figure S7.

KEY RESOURCES TABLE

REAGENT or RESOURCE	SOURCE	IDENTIFIER
Antibodies		
APC anti-CD31	BD Biosciences	Catalogue #: 551262; RRID:AB_398497
APC anti-CD45	BD Biosciences	Catalogue #: 559864; RRID:AB_398672
APC anti-TER119	BD Biosciences	Catalogue #: 557909; RRID:AB_398635
Chicken anti-Keratin14	Gift from J. Segre	N/A
FITC anti-CD49f	Bio-Legend	Catalogue #: 555735; RRID:AB_396078
FITC anti-CD49f	Bio-Legend	Catalogue #: 102205; RRID:AB_2794263
Goat anti-Chicken Rhodamine IgY Red-X	Jackson Immuno Research	Catalogue #: 103–295-155; RRID:AB_2337388
Goat anti-Rabbit IgG Alexa Fluor 488	Life Technologies	Catalogue #: A11008; RRID:AB_143165
Mouse Anti-Human IgG (H+L)	Santa Cruz Biotechnology	Catalogue #: SC-2027; RRID:AB_737197
PE/Cy-7 anti-CD326	Bio-Legend	Catalogue #: 118215; RRID:AB_1236477
Rabbit anti-aSMA	Abcam	Catalogue #: ab5694; RRID:AB_2223021
Rabbit anti-Ki-67	Cell Signaling	Catalogue #: 9129, RRID:AB_2687446
Rabbit Anti-YAP1	Cell Signaling	Catalogue #: 8418, RRID:AB_10950494
Rabbit anti-Zeb1	Novus Biologicals	Catalogue #: NBP1–88845; RRID:AB_11038094
Rabbit anti-Zeb1	Santa Cruz	Catalogue #: SC-25388; RRID:AB_2217979
Chemicals/peptides, and recombinant proteins		
Affi-Gel Blue Gel	Bio-Rad Laboratories	Catalogue #: 1537301
BIO	Millipore Sigma	Catalogue #: B1686
Heparin	Stem Cell Technologies	Catalogue #: 7980
Hoechst 33342	Life Technologies	Catalogue #: H3570
Hydrocortisone	Calbiochem	Catalogue #: 386698
Insulin	Sigma	Catalogue #: 16634
Prolactin	Sigma	Catalogue #: L66520
Pyronin Y	Santa Cruz	Catalogue #: 92–32-0
Recombinant Human EGF	Millipore	Catalogue #: 01–107
Recombinant Human FGF-2	Pepro-Tech	Catalogue #: 100–18B

REAGENT or RESOURCE	SOURCE	IDENTIFIER
Recombinant Human Noggin	Fisher Scientific	Catalogue #: 50–399-006
Recombinant Human Wnt3a	R&D Biosystems	Catalogue #: 5306-WN
Recombinant Mouse DKK1	R&D Biosystems	Catalogue #: 5897-DK-010
Recombinant Mouse EGF	Invitrogen	Catalogue #: PMG-8043
Recombinant Mouse Respondin 1 (RSPO1)	R&D Biosystems	Catalogue #: 3474-RS
ROCK Inhibitor (Y-27632)	Millipore Sigma	Catalogue #: SCM075
Critical commercial assays		
High Capacity cDNA Kit	Thermo Fisher	Catalogue #: 4368814
Luciferase Assay System	Promega	Catalogue #: E1500
Quick-RNA Microprep	Zymo Research	Catalogue #: R1050
SMART-seq V4 ultra low input RNA kit	Takara Bio	Catalogue #: 634892
SSO Adv. Univ. SYBR Green Super Mix	Bio-Rad	Catalogue #: 172–5271
Deposited data		
Single Cell RNA-seq data (10x)	This paper	GEO: GSE155636
Single Cell RNA-seq data (Fluidigm C1)	This paper	GEO: GSE155636
Bulk Cell RNA-seq data (G0/G1 basal cells)	This paper	GEO: GSE188781
Bulk Cell RNA-seq data (MCF-10A)	This paper	GEO: GSE70551
Experimental models: Organisms/strains		
293T cells	Gift of Haoping Liu Laboratory	N/A
3T3 cells	ATCC	Catalogue #: CRL-1658
B6N.Cg-Tg(KRT14-cre)1Amc/J	Jackson Laboratory	Catalogue #: 18964
C57BL/6J	Jackson Laboratory	N/A
Gt(ROSA)26Sor$^{tm4(ACTB-tdTomato,-EGFP)Luo}$	Jackson Laboratory	Catalogue #: 7676
MCF-10A	ATCC	Catalogue #: CRL-10317
MDA-MB-231	ATCC	Catalogue #: HTB-26
Ovol2$^{flox/flox}$	Watanabe et al. (2014)	NA
Zeb1$^{flox/flox}$	Brabletz et al. (2017)	N/A

REAGENT or RESOURCE	SOURCE	IDENTIFIER
Oligonucleotides		
Oligos for genotyping, RT-qPCR, and ChIP-PCR (Table S6)	Life Technologies	N/A
Oligos for cloning (Table S6)	Eurofins Genomics	N/A
$Zeb1^{flox/flox}$	Brabletz et al. (2017)	N/A
0.25% Trypsin	Gibco	Catalogue #: 25200
10x Chromium System	10x Genomics	N/A
40uM Mesh	SWiSH	Catalogue #: TC70-MT-1
Agilent Bio Analyzer 2100	Agilent	N/A
CFX96 RT-qPCR system	Bio-Rad	N/A
Collagenase	Sigma	Catalogue #: C9891
Dispase II	Stem Cell Technologies	Catalogue #: 7913
DMEM: F12 (1:1)	Thermo Fisher	Catalogue #: 12500–062
DMEM/F12	Stem Cell Technologies	Catalogue #: 26254
DNAse I	Sigma	Catalogue #: DN25
Epicult-B Medium	Stem Cell Technologies	Catalogue #: 5610
FACSAria Cell Sorter	Becton Dickenson UK	N/A
Fetal Bovine Serum	Omega Scientific	Catalogue #: FB-02
Fluidigm C1 Chip	Fluidigm	Catalogue #: 100–5760
Fluidigm C1 Suspension Reagent	Fluidigm	Catalogue #: 100–5315
Fluidigm C1 System	Fluidigm	N/A
HBSS	Gibco	Catalogue #: 14025134
HEPES	Millipore Sigma	Catalogue #: H3375
HiSeq-4000	Illumina	N/A
Hyaluronidase	Sigma	Catalogue #: H3506
Keyence BZ-X710 Microscope	Keyence Corp.	N/A
Matrigel Membrane Matrix	BD Biosciences	Catalogue #: XB-40230
NanoDrop ND-1000	Thermo Fisher	N/A
Novocyte	ACEA Biosciences	N/A
pCB6+ Vector	Gift of Elaine Fuchs Laboratory	N/A
pHIV-ZsGreen	AddGene	Catalogue #: 18121

REAGENT or RESOURCE	SOURCE	IDENTIFIER
Polystyrene Plates	Corning	Catalogue #: 3473
RBC Lysis Buffer	Sigma	Catalogue #: R7757
RNA Lysis Buffer	Zymo Research	Catalogue #: R1050
TrypLE Select	Gibco	Catalogue #: 12605–010
Universal SYBR Green Super mix	Bio-Rad	Catalogue#: 172–5271
Zeiss LSM 700 Confocal Microscope	Zeiss	N/A